Long-term changes and variability in a transient simulation with a chemistry-climate model employing realistic forcing

M. Dameris, V. Grewe, M. Ponater, R. Deckert, V. Eyring, F. Mager, S. Matthes, C. Schnadt, A. Stenke, B. Steil, et al.

HAL Id: hal-00303900

https://hal.science/hal-00303900

Submitted on 18 Jun 2008

**Atmospheric
Chemistry
and Physics
Discussions**

ACPD

5, 2297–2353, 2005

**Variability in a
transient CCM
simulation**

M. Dameris et al.

Long-term changes and variability in a transient simulation with a chemistry-climate model employing realistic forcing

**M. Dameris[1], V. Grewe[1], M. Ponater[1], R. Deckert[1], V. Eyring[1], F. Mager[1,4],
S. Matthes[1], C. Schnadt[1,5], A. Stenke[1], B. Steil[2], C. Brühl[2], and M. A. Giorgetta[3]**

[1]Institut für Physik der Atmosphäre, DLR-Oberpfaffenhofen, Wessling, Germany
[2]Max-Planck-Institut für Chemie, Mainz, Germany
[3]Max-Planck-Institut für Meteorologie, Hamburg, Germany
[4]now at: University of Cambridge, Centre for Atmospheric Science, Department of Geography, Cambridge, United Kingdom
[5]now at: ETH Zürich, Institut für Atmosphäre und Klima, Zürich, Switzerland

Title Page

Abstract | Introduction

Conclusions | References

Tables | Figures

◄◄ | ►►

◄ | ►

Back | Close

Full Screen / Esc

Print Version

Interactive Discussion

EGU

Variability in a transient CCM simulation

M. Dameris et al.

Abstract

A transient simulation with the interactively coupled chemistry-climate model (CCM) E39/C has been carried out which covers the 40-year period between 1960 and 1999. Forcing of natural and anthropogenic origin is prescribed where the characteristics

5   are sufficiently well known and the typical timescales are slow compared to synoptic timescale so that the simulated atmospheric chemistry and climate evolves under a "slowly" varying external forcing. Based on observations, sea surface temperature (SST) and ice cover are prescribed. The increase of greenhouse gas and chlorofluro-carbon concentrations, as well as nitrogen oxide emissions is taken into account. The

10   11-year solar cycle is considered in the calculation of heating rates and photolysis of chemical species. The three major volcanic eruptions during that time (Agung, 1963; El Chichon, 1982; Pinatubo, 1991) are considered. The quasi-biennial oscillation (QBO) is forced by linear relaxation, also known as nudging, of the equatorial zonal wind in the lower stratosphere towards observed zonal wind profiles. Beyond a reasonable repro-

15   duction of mean parameters and long-term variability characteristics there are many apparent features of episodic similarities between simulation and observation: In the years 1986 and 1988 the Antarctic ozone holes are smaller than in the other years of the respective decade. In mid-latitudes of the Southern Hemisphere ozone anomalies, especially in 1985, 1989, 1991/1992, and 1996, resemble the corresponding observa-

20   tions. In the Northern Hemisphere, the first half of the 1990s is dynamically quiet, no stratospheric warming is found for a period of at least 6 years. As observed, volcanic eruptions strongly influence dynamics and chemistry, though only for few years. Obviously, planetary wave activity is strongly driven by the prescribed SST and modulated by the QBO. Preliminary evidence of realistic cause and effect relationships strongly

25   suggest that detailed process-oriented studies will be a worthwhile endeavour.

1. Introduction

In recent years, more and more results of interactively coupled chemistry-climate models (CCMs) have become available (e.g. Rozanov et al., 2001; Austin, 2002; Nagashima et al., 2002; Pitari et al., 2002; Schnadt et al., 2002; Steil et al., 2003; Manzini et al., 2003). First of all, they have been developed to examine the feedback between dynamical, physical, and chemical processes in the atmosphere, with a particular focus on the upper troposphere and stratosphere. The primary purpose of CCMs is to support analyses of long-term observations and to explain recent changes and variability of the chemical composition and dynamics. Like other complex model systems, CCMs must carefully be checked with respect to their abilities and deficiencies to describe present and recent atmospheric conditions before they can be applied for reliable estimates of future changes.

Currently, there are two concepts to perform numerical experiments with CCMs: Firstly, so-called time-slice experiments are well suited to investigate the internal variability of the coupled chemistry-climate system and to indicate and estimate the significance of specific changes of certain parameters or processes in past, present or future climate states with respect to a reference state. Such simulations are carried out with fixed boundary conditions given for a specific year, for example, concentrations of greenhouse gases (GHGs), emissions of natural and anthropogenic source gases, sea surface temperatures (SSTs), etc., to investigate the corresponding "equilibrium climate". The comparison of time-slice simulations among each other is favourable to identify and interpret long-term temporal developments, e.g. pattern changes, in case that the assessment of statistical significance poses a problem. Secondly, transient model simulations, which involve gradual changes in GHGs and other boundary conditions, allow a more direct comparison with the corresponding continuous behaviour of the observed atmosphere. In particular, non-persistent perturbations of the stationary or slowly varying behaviour of the real atmosphere can be included in the simulation for a more detailed model evaluation. Both strategies of model simulations lead to useful

Title Page

Abstract	Introduction
Conclusions	References
Tables	Figures

◄◄ ►►

◄ ►

Back Close

Full Screen / Esc

Print Version

Interactive Discussion

EGU

results to better understand atmospheric processes. This is demonstrated by a considerable number of papers which have recently been published (e.g. Rozanov et al., 2001; Austin, 2002; Nagashima et al., 2002; Pitari et al., 2002; Schnadt et al., 2002; Steil et al., 2003; Manzini et al., 2003). A number of examples of concerning strengths and weaknesses of CCMs were discussed in Austin et al. (2003) where the results of different CCMs have been compared with observations and each other. The studies mentioned above have concentrated on the stratosphere, other ones have the main focus on the troposphere (e.g. Wang and Prinn, 1999; Johnson et al., 1999; Grewe et al., 2001a). All these CCM studies have in common that they focus on specific causes and effect relationships with respect to atmospheric chemistry and dynamics, but rarely try to investigate the complete system.

It is the central objective of this paper to investigate and discuss the results of a transient simulation with a state-of-the-art CCM. While E39/C simulates tropospheric and lower stratospheric processes as components of equal importance, the focus of our analysis is on the upper troposphere and lower stratosphere. Moreover, we have tried to include a comprehensive set of external forcings on variability and trends in order to allow a fair comparison with observations and to assess the capability to reproduce the development of the real atmosphere. To our knowledge, this is one of the first transient CCM simulations which, beyond trends in trace gas emissions and concentrations, also considers the observed sea surface temperature (SST) variability, the impact of large volcanic eruptions, the 11-year solar cycle effect, and the quasi-biennial oscillation (QBO). They all have significant impacts on processes which determine the dynamics and chemistry of the atmosphere. The aim of this investigation is to identify and better understand the importance of external forcings on climate and chemical composition. For example, a key question is the deterministic behaviour of a non-linear model system to such forcings. A detailed comparison of model results and data products derived from long-term observations is presented to advance our understanding for answering the above questions.

In the following section a brief description of the model and the experimental set-

[ACPD](#)

5, 2297–2353, 2005

Variability in a transient CCM simulation

M. Dameris et al.

Title Page

Abstract | Introduction

Conclusions | References

Tables | Figures

◀ | ▶

◀ | ▶

Back | Close

Full Screen / Esc

Print Version

Interactive Discussion

EGU

up is given. Section 3 concentrates on long-term changes (trends) in observations and model data. The variability due to prescribed forcings (i.e. volcanic eruptions, QBO, solar cycle, SSTs) are discussed in Sect. 4. The results discussed in this paper concentrate on the upper troposphere and lower stratosphere region (UTLS), which is conditioned by the model domain. The last section gives some conclusions and an outlook.

2. Model description and experimental set up

2.1. The CCM ECHAM4.L39(DLR)/CHEM

In this study, the interactively coupled CCM ECHAM4.L39(DLR)/CHEM (hereafter: E39/C) is used for a transient model simulation covering the time period from 1960 to 1999. The model system has been applied previously for several investigations, but there results from time-slice runs were used exclusively. A basic description about E39/C is given in detail by Hein et al. (2001), Grewe et al. (2001b), and Schnadt et al. (2002). In the following, the setup of E39/C is only briefly summarised.

The horizontal resolution of E39/C is T30, i.e. dynamical processes have an isotropic resolution of about 670 km. The corresponding Gaussian transform latitude-longitude grid, on which the model physics, chemistry, and tracer transport are calculated, has a mash size of 3.75°×3.75°. In the vertical, E39/C has 39 layers from the surface up to the top layer of the model centred at 10 hPa (Land et al., 2002). The chemistry model CHEM (Steil et al., 1998) is based on a generalised improved family concept which has three upgrades: 1) get rid of the general use of steady state; b)consider coupling between families by solving combined families; and c) definitions of families for transport and chemistry are different. CHEM describes relevant stratospheric and tropospheric O_3 related homogeneous chemical reactions and heterogeneous chemistry on PSCs and sulphate aerosols, it does not include bromine chemistry. The model version used in the present study includes updates of the rate coefficients of gasphase

Variability in a transient CCM simulation

M. Dameris et al.

Title Page

Abstract	Introduction
Conclusions	References
Tables	Figures

◀◀ ▶▶

◀ ▶

Back Close

Full Screen / Esc

Print Version

Interactive Discussion

EGU

reactions JPL (2000). Two heterogeneous reactions on stratospheric aerosol have been added ($ClONO_2+HCl\rightarrow Cl_2+HNO_3$ and $HOCl+HCl\rightarrow Cl_2+H_2O$). The transport of chlorine components has been improved by transporting both total chlorine and the partitioning of chlorine species, to minimise numerical diffusion in regions with lower vertical resolution. The net heating rates and photolysis rates in E39/C are calculated using the actual three-dimensional (3-D) distributions of the radiatively active gases O_3, CH_4, N_2O, H_2O, and CFCs, and the 3-D cloud distribution. The model climatology has been extensively validated; specifically, analyses on the model's performance in the Arctic stratosphere have been carried out (Hein et al., 2001; Austin et al., 2003).

The photolysis at solar zenith angles (SZAs) larger than 87.5° has been implemented into E39/C to account for the effects of twilight stratospheric ozone chemistry. Lamago et al. (2003) showed that the temperature, as well as ozone fields particularly in polar regions are more realistic when SZAs up to 93° are considered. The photolysis frequencies for SZA larger than 87.5° are parameterised multiplying the photolysis rate at 87.5° with an exponential correction factor for SZAs up to 93° (for details see Lamago et al., 2003).

The lightning parameterisation developed by Price and Rind (1992), which was used in E39/C so far to account for NO_x emissions from lightning, has been replaced by an improved parameterisation developed by Grewe et al. (2001b). Grewe et al. relate the flash rate to the vertical air mass exchange within a convective cloud. A comparison of flash frequencies calculated by E39/C and derived from the Optical Transient Detector (OTD) observations onboard the MicroLab satellite, showed a qualitatively and quantitatively reasonable agreement (Kurz and Grewe, 2002). The parameterisation takes into account intra-cloud and cloud to ground lightning (Price and Rind, 1993) and uses effective NO_x emission profiles (Pickering et al., 1998). The annual mean emission rate over the 40-year simulation period amounts to 5.16 Tg(N)/a.

Variability in a transient CCM simulation

M. Dameris et al.

Title Page

Abstract | Introduction

Conclusions | References

Tables | Figures

◄ | ►

◄ | ►

Back | Close

Full Screen / Esc

Print Version

Interactive Discussion

EGU

2.2. Design of the transient simulation

The transient integration of E39/C is designed to represent the development during the period from 1960 to 1999. A spin-up of ten years for stationary conditions of the late 1950s preceded the actual transient part of the experiment. The simulation aims to reproduce the effect of natural, as well as anthropogenic forcings. The natural factors considered in the transient integration are the 11-year solar cycle, the QBO, and the chemical and direct radiative effects of the major volcanic eruptions of Agung in 1963, El Chichon in 1982, and Mt. Pinatubo in 1991. The anthropogenic influence is represented by specifying atmospheric concentrations of the most important GHGs, chlorofluorocarbons (CFCs), and nitrogen oxide emissions. However, part of the anthropogenic effect is also accounted for by using an SST development prescribed from observations.

Table 1 gives an overview of the boundary conditions for the transient simulation. The SSTs are prescribed as monthly means following the global sea ice and sea surface temperature (HadISST1) data set provided by the UK Met Office Hadley Centre (Rayner et al., 2003). These data are based on blended satellite and in situ observations. A few gaps in sea ice coverage caused by interpolation to the model grid have been removed by a careful consistency check.

Both chemical and direct radiative effects of enhanced stratospheric aerosol abundance from large volcanic eruptions are considered. For heterogeneous reactions covered in the chemistry module, sulphate aerosol surface area densities partly had to be approximated from observations as follows: The original data set consists of monthly and zonally averaged sulphate aerosol surface area densities (WMO, 2003). It was deduced from satellite-based extinction measurements (SAGE I, SAGE II, SAM II, and SME), as has been described in Jackman et al. (1996), using the methodology of Rosenfield et al. (1997). The Agung eruption in 1963 is not covered by this data set. As a remedy, the well-documented years following the eruption of Mt. Pinatubo (1991–1994) have been adopted and associated with the period 1963–1966 with modifica-

[ACPD](#)

5, 2297–2353, 2005

Variability in a transient CCM simulation

M. Dameris et al.

Title Page	
Abstract	Introduction
Conclusions	References
Tables	Figures
◀◀	▶▶
◀	▶
Back	Close
Full Screen / Esc	
Print Version	
Interactive Discussion	

[EGU](#)

Variability in a transient CCM simulation

M. Dameris et al.

tions based on published results to account for differences in total mass of sulphate aerosols inside the stratosphere, in maximum height of the eruption plumes, and in the volcanoes' geographical location (e.g. Sato et al., 1993; Andronova et al., 1999; Robock, 2000). Above the maximum vertical extent of Agung's eruption plume the an-

⁵ nual mean of 1979 has been incorporated. By 1979 the total mass of stratospheric sulphate aerosol had probably returned to its background value, being maintained by a permanent supply of tropospheric sulphur species (Junge et al., 1961; Mc Cormick et al., 1995). For the time periods 1960–1962 and 1968–1978 the annual mean of 1979 has been adopted, and for the period 1996–1999 the annual mean of 1995 has

¹⁰ been used. Additionally, the data set has been interpolated linearly both from 177 to 16 vertical levels, and from 18 latitudes to 48 latitudes.

Eruption-related radiative heating is implemented in E39/C using pre-calculated monthly and zonally mean net heating rates. These rates were available from a previous ECHAM4(T42)/L19 (L19=19 vertical layer) Pinatubo sensitivity experiment, which

¹⁵ was forced by a realistic space-time dependent aerosol distribution (Kirchner et al., 1999). The original data set extends from July 1991 to April 1993. Thus, only part of the eruption-influenced time span was available, e.g. June 1991 (month of eruption) is missed. Therefore, for June 1991 the radiative forcing has been taken as $0.5 \times$ July 1991 values, and an exponential decay has been adopted in the period from May 1993

²⁰ to July 1993. With regard to the Agung and El Chichon eruptions, the Pinatubo net heating rates have also been used without major changes, because there were strong hints for a similar radiative heating (e.g. Labitzke, 1994). Finally, the data have been interpolated from L19 to L39 (i.e. number of vertical layers in E39/C).

The QBO is generally described by zonal wind profiles measured nearby the equator.

²⁵ Radiosonde data from Canton Island (1953–1967), Gan/Maledives (1967–1975) and Singapore (1976–2000) have been used to develop a time series of monthly mean zonal winds at the equator (Naujokat, 1986; Labitzke et al., 2002). This data set covers the lower stratosphere up to 10 hPa. It is used to assimilate the QBO in E39/C, such that the QBO is synchronised with other external inter-annual variations prescribed in

Variability in a transient CCM simulation

M. Dameris et al.

EGU

this experiment. For the assimilation it is assumed that the QBO is zonally symmetric and that it has a Gausian half width of about 12° latitude around the equator. The QBO is forced in E39/C by a linear relaxation of the predicted zonal wind towards the constructed QBO time series, which follows the observed zonal wind profile (Giorgetta and Bengtsson, 1999). This assimilation is applied equatorwards of 20° latitude from 90 hPa up to the highest layer of the model centred at 10 hPa. The relaxation time scale has been set to 7 days within the QBO core domain. Outside of this core domain the time scale depends on latitude and pressure (Giorgetta and Bengtsson, 1999). Figure 1 shows the results of the assimilated monthly mean zonal winds of the E39/C run for the time period 1960 to 1999. The assimilated QBO compares well with the observed phase state and the observed amplitudes of the westerlies and easterlies (Giorgetta and Bengtsson, 1999, their Fig. 1).

The influence of the 11-year solar cycle on photolysis rates is parameterised according to the intensity of the 10.7 cm radiation of the sun (data available at: http://www.drao.nrc.ca/icarus/www/daily.html). Table 2 gives the values of the extra-terrestrial fluxes in different spectral intervals assumed for high (i.e. these values represent the year 1991) and low solar activity used at the upper boundary of E39/C. The 1991 solar maximum values are employed as reference values for the calculation of respective values for maximum solar activity of the other solar cycles which are considered in the transient run, i.e. 1958, 1969, and 1980. These values are scaled with the intensity of the 10.7 cm flux of the corresponding years. Photolysis rates are calculated in 8 spectral intervals (Landgraf and Crutzen, 1998). The spectral distribution of changes in extra-terrestrial flux is based on investigations presented by Lean et al. (1997). The ozone columns above the model top (i.e. centred at 10 hPa) are considered by a seasonally dependent climatology which is taken from HALOE observations. It must be mentioned that those climatological values are an average of 6 years only and therefore do not consider changes due to the solar cycle. The impact of solar activity changes on short-wave radiative heating rates is prescribed due to changes of the solar constant (see Table 2). Short-wave radiative heating rates are considered in

two spectral intervals (Morcrette, 1999; Fouquart and Bonnel, 1980), respecting continuum scattering, grey absorption, water vapour and uniformly mixed gases transmission functions and ozone transmission.

Continuously changing mixing ratios of the most relevant greenhouse gases (CO_2, N_2O, CH_4) are prescribed, CO_2 for the entire model domain, the others at the Earth's surface according to Hein et al. (1997) and IPCC (2001; see Fig. 2). Carbon monoxide (CO) mixing ratio is kept constant (Hein et al., 1997). Natural and anthropogenic nitrogen oxide (NO_x=NO+NO_2) emissions at the Earth's surface, and NO_x emission from lightning and air traffic are considered. In the following a brief summary of the individual NO_x emission sources and their temporal changes is given.

The horizontal distribution of NO_x from industry is based on Benkovitz et al. (1996) and its temporal development has been adapted to match the IPCC (2001) values. The increase of the emission rates from 1960 to 1999 are assumed to be almost constant around 1.6%/year IPCC (1999). Anthropogenic NO_x emissions include those from surface transportation as an individual component (Matthes, 2003), which contributes approximately 30% to the total industry emissions (see also Matthes et al., 2005[1]). Ship emissions have been removed from the global dataset (Benkovitz et al., 1996). Instead, a more sophisticated ship emission inventory with 1993 annual global NO_x emissions of 3.08 Tg(N) is used as the basic data set (Corbett et al., 1999). Trend estimates of NO_x emissions from international shipping for the time period 1960 to 2000 have been adopted from Eyring et al. (2004)[2]. Based on these assumptions, the annual global NO_x emissions from ships for the years 1960 to 1999 amount to 1.17 Tg(N) and 3.28 Tg(N), respectively. Aircraft NO_x emissions are based on a data set representing 1992 (Schmitt and Brunner, 1997). Trends previous to 1992 are extrapolated

---

[1] Matthes, S., Grewe, V., Sausen, R., and Roelofs, G.-J.: Global impact of road traffic emissions on the chemical composition of the atmosphere, Atmos. Chem. Phys. Discuss., submitted, 2005.

[2] Eyring, V., Köhler, H. W., van Aardenne, J., and Lauer, A.: Emissions from international shipping. Part 1: The last 50 years, J. Geophys. Res., submitted, 2004.

EGU

using IPCC (1999). For the period 1992 to 1999 an exponential interpolation has been applied. The aircraft NO_x emissions for the years 1960 to 1999 amount to 0.10 Tg(N) and 0.71 Tg(N).

Nitrogen oxide emissions from biomass burning are based on Hao et al. (1990) and are revised using ASTR fire counts (David Lee, pers. comm. 2004). The trend rates are roughly 0.3%/year (IPCC, 1999). The global NO_x soil emissions by micro-biological production are assumed to be constant over the four decades of the transient simulation. They are taken from Yienger and Levy (1995). As mentioned above, lightning NO_x emissions are calculated interactively, based on the parameterised mean mass flux in the updraft of deep convective clouds (see previous section), resulting in a mean annual emission of 5.16 Tg(N). The interannual variability ranges between 4.81 and 5.42 Tg(N)/a and the seasonal cycle varies with ±14%. We anticipate that no systematic trend of lightning NO_x emissions is found over the 40-year transient simulation.

To take into account exchange processes from the upper stratosphere, upper boundary conditions are adopted for the two families ClX and NO_y at 10 hPa ($ClX=HCl+ClONO_2+ClO_x$, $ClO_x=Cl+ClO+ClOH+2\cdot Cl_2O_2+2\cdot Cl_2$, $NO_y=NO_x+N+NO_3+2\cdot N_2O_5+HNO_4+HNO_3$). They largely determine lower stratospheric nitrogen oxide and chlorine concentrations. Monthly mean concentrations are taken from results of the two-dimensional (2-D) middle atmosphere model of Brühl and Crutzen (1993), which also considers the effects of the 11-year solar cycle. For example, the NO_y values prescribed at the model's upper boundary fluctuate according to solar activity. Additionally, since CFCs are not explicitly transported by E39/C, they are included based on results derived from the 2-D model (depending on latitude and altitude), and serve as a source for total chlorine (Cl_y) by photolysis, within the model domain.

The development of CFC concentrations is prescribed in agreement with most recent assumptions (WMO, 2003). Stratospheric Cl_y has been calculated as sum of the simulated ClO_x, $ClONO_2$, HCl fields, and chlorine from the prescribed CFC fields (see Fig. 2). Its temporal evolution reflects the observed development (WMO, 2003, their

Figs. 1–7).

3. Long-term trends

In this section climatic variability and trends of key parameters will be presented and discussed with respect to corresponding observations.

5 3.1. Ozone

Figure 3 shows the development of monthly and zonal mean total ozone for the whole simulation period. It indicates the well-known features, e.g. highest ozone values in northern spring time which is highly variable from year-to-year, low ozone values in the tropics with a small seasonal cycle and little interannual variability, a relative ozone
10 maximum in mid-latitudes of the Southern Hemisphere in late winter/early spring, and a minimum ozone column above the south polar region. The ozone hole appears for the first time in the year 1982 in E39/C, which is in agreement with observations (Chubachi, 1985; Farman et al., 1985). Another interesting feature is the absence of total ozone values above 475 DU in the Northern Hemisphere during the late 1980s and
15 the first half of the 1990s. This indicates a period of at least six years without distinct mid-winter warmings of the stratosphere. There is no other comparable episode in the 40-year simulation. This agrees with the evolution of the real atmosphere, where northern winters from 1989/1990 to 1996/1997 show no major stratospheric warming events (e.g. Naujokat and Pawson, 1996; Naujokat et al., 1997; Pawson and Naujokat,
20 1999) resulting in significant springtime ozone losses during these years (e.g. Rex et al., 2004).
   In order to get a closer insight into regional and temporal patterns in the interannual variability of ozone changes, Fig. 4 shows total ozone anomalies for the whole model simulation with respect to mean values based on the years 1964 to 1980. The fea-
25 tures discussed above can easily be identified again, especially that ozone depletion

Variability in a transient CCM simulation

M. Dameris et al.

Title Page

Abstract | Introduction

Conclusions | References

Tables | Figures

◄◄ | ►►

◄ | ►

Back | Close

Full Screen / Esc

Print Version

Interactive Discussion

EGU

starts first in high latitudes of the Southern Hemisphere and that the reduction of the ozone layer occurs later in the Northern Hemisphere and the tropical region. But there are also some additional eye-catching features: For example, as identified in observations (e.g. Bojkov and Fioletov, 1995), the ozone holes in the years 1986 and 1988 are

5 clearly smaller than in the respective year before. A closer inspection of the dynamics of the polar vortices in E39/C during these years indicate in both cases that the vortex is less stable and displaced from the polar region towards lower latitudes, which is very similar to the observed dynamical behaviour of the polar vortices in 1986 and 1988. There are a number of other interesting similarities in mid-latitudes of the Southern

10 Hemisphere, i.e. modelled positive and negative ozone anomalies which nicely match observations, in particular in 1985, 1989, 1991, 1992, and 1996 (see Bojkov and Fioletov, 1995, their Plate 1). A process related discussion about possible reasons for these consistencies with observations will be given in the next section. Looking into the tropics, there is distinct variability clearly reflecting the QBO signal; this is discussed in

15 more detail in Sect. 4.2.

Before looking more closely at the long-term variability and changes (trends) calculated by the model, we take a look at the systematic bias of total ozone in E39/C. Figures 5a and 5b show 20-year mean climatological total ozone values derived from the E39/C simulation, i.e. the 1960s and 1970s, and the 1980s and 1990s. The clima-

20 tology derived from measurements of the TOMS instrument for the years 1980 to 1999 is displayed in Fig. 5c. A comparison of Figs. 5b and 5c indicates that E39/C is able to reproduce the main features (e.g. regional distribution, seasonal cycle) in qualitative agreement with TOMS observations. In the Northern Hemisphere and the tropics, the model calculates total ozone values which are about 10 to 15% higher than those values derived from TOMS. These model results confirm the findings of the E39/C time-

25 slice experiments (e.g. Hein et al., 2001). However, in the Southern Hemisphere the model shows an improved behaviour with respect to former studies with E39/C: The absolute total ozone values are in overall agreement with TOMS, merely the ozone hole season in E39/C lasts slightly longer and the mid-latitude ozone maximum is somewhat

Variability in a transient CCM simulation

M. Dameris et al.

Title Page

Abstract	Introduction
Conclusions	References
Tables	Figures

◄ | ►|

◄ | ►

Back | Close

Full Screen / Esc

Print Version

Interactive Discussion

EGU

higher. This model improvement can partly be attributed to the fact that large SZAs are now considered for the calculation of photolysis rates which has a clear impact on the model behaviour, in particular in the Southern Hemisphere (Lamago et al., 2003).

Figure 5d displays the simulated differences between the two E39/C climatologies affected by the ozone hole (1980–1999; Fig. 5b) and the preceding era (1960–1979; Fig. 5a). Since the 1960s and 1970s represent a climatological mean state of an almost unperturbed episode, this climatology can be taken as a basis to derive trends from 1980 onwards. As anticipated, largest changes are found in the south polar region during spring time, where 60 DU less ozone is calculated in the second half of the transient simulation compared with the first half. This amounts to an ozone reduction of about 20% per decade. Especially in the 1990s, ozone decreases steadily with more than 40% less ozone at the end of the century compared to 1980. These estimates agree well with numbers derived from observations. For example, based on TOMS-data for the years between 1978 and 1994, Mc Peters et al. (1996) estimated the ozone loss to be 20%/decade.

Also in the Northern Hemisphere, the trend pattern and absolute numbers agree with analyses from measurements: McPeters et al. found an ozone reduction in northern spring of about 6%/decade. The model shows a decrease of about 25 DU (Fig. 5d), which relates to a trend of about 5% per decade. A small increase (i.e. less than 7 DU) in total ozone is simulated by E39/C in northern summer. It is caused by an increase of tropospheric ozone concentration whereas at the same time no clear change is simulated in the lower stratosphere (see Fig. 6b). The vertical ozone distribution (Fig. 6a) and its seasonal changes are very similar with results derived from E39/C time-slice experiments (e.g. Hein et al., 2001) which are in reasonable agreement with observations (e.g. Fortuin and Kelder, 1998). The simulated ozone changes throughout the four decades are almost everywhere statistically significant: Ozone mixing ratios have increased during equinox (MAM, SON) in the middle troposphere of the Northern Hemisphere by more than 10 ppbv, whereas in the lower stratosphere a general decrease is evident, in particular in the polar Southern Hemisphere spring time (SON). The in-

Variability in a transient CCM simulation

M. Dameris et al.

Title Page

Abstract	Introduction
Conclusions	References
Tables	Figures

◄◄ ►►

◄ ►

Back Close

Full Screen / Esc

Print Version

Interactive Discussion

EGU

crease of tropospheric ozone mixing ratios are due to the increased NO_x emissions (e.g. Grewe et al., 2001b) whereas stratospheric ozone depletion is a consequence of increased halogen loading and temperature decrease in the stratosphere due to an increased abundance of GHGs (e.g. Schnadt et al., 2002).

5   3.2.   Temperature and zonal wind

Climatologies of temperature and zonal mean wind fields for the 1960s and their changes throughout the four decades, as simulated by E39/C, are displayed in Figs. 7 and 8. The mean fields for the 1960s (Figs. 7a and 8a) are satisfactorily reproduced compared with NCEP re-analysis data (not shown) as well as climatological mean val-
10   ues for the 1990s (see also Pawson et al., 2000). Sub-tropical and polar night jets are clearly distinguishable, i.e. a transition zone with reduced wind speed is found in both hemispheres for all seasons. A continuous model problem arises in the Southern Hemisphere winter and spring months, where E39/C is calculating too low temperatures in the entire polar lower stratosphere. Therefore, the climatological mean polar
15   vortex is too strong and stable (Fig. 8a, see also Hein et al., 2001; Austin et al., 2003). Another discrepancy has been identified in the zonal mean stratospheric wind fields in the summer hemispheres. The summer vortices in both hemispheres are slightly shifted towards the tropics, a wind reversal in upper model layers at higher latitudes is missed. No easterlies winds are simulated poleward of 55° S in the Southern Hemi-
20   sphere (DJF) and in the Northern Hemisphere (JJA), the calculated easterlies at polar latitudes are too weak. The structure of temperature changes between the 1960s and 1990s (i.e. increase of tropospheric temperature, decrease of stratospheric temperature) partly arises from the increase in greenhouse gas concentrations, in the polar lower stratosphere it mostly reflects the decrease of ozone (Fig. 7b). Strongest temper-
25   ature decrease is seen in the Southern Hemisphere polar lower stratosphere in SON (up to −10 K at 30 hPa) and DJF (up to −6 K at around 70 hPa), the time during and after the appearance of the ozone hole, which is in good agreement with assessments derived from observations (e.g. Randel and Wu, 1999). A statistically significant tem-

EGU

perature increase of more than 1 K is found in the (sub-)tropical upper troposphere whereas a (non significant) cooling is calculated in the lower tropical stratosphere. The latter finding is in qualitative agreement with analyses of observations which also indicate a cooling trend with numbers ranging from −0.3 to −1.4 K per decade (e.g. WMO, 1999). The picture is rather unclear in the tropical tropopause region. For example, temperature trends derived from observations estimated at 100 hPa (WMO, 1999) range from +0.3 to −0.5 K. Certainly, this is a difficult region to obtain a clear trend signal, because it is the transition layer with a warming below and a cooling above. As many other models, E39/C simulates a warming in the upper troposphere, which maximises at 250 hPa, but this is not in agreement with radiosonde temperature data which indicate a cooling (e.g. Parker et al., 1997). Long-term temperature changes at middle and higher latitudes of the Northern Hemisphere middle troposphere (500 hPa) derived from E39/C (Fig. 7b) varies between +0.5 K (JJA) and +1.0 K (DJF), which is less than detected at the Meteorological Observatory Hohenpeissenberg, station of the German Weather Service (MOHp; 47.8° N, 11° E) where an increase of +0.7±0.3 K per decade has been found since 1967 (Steinbrecht et al., 1998). In general, the long-term temperature changes derived from the E39/C transient model simulation confirm recent estimates from E39/C time-slice experiments (i.e. 1980 and 1990 conditions) presented also in Shine et al. (2003).

Corresponding changes of the zonal mean wind field are shown in Fig. 8b. The statistically significant increase of the zonal mean wind speed of up to 6 m/s in the Southern Hemisphere lower stratosphere during spring (SON) and summer months (DJF) reflect the ozone hole formation and the corresponding decrease of polar stratospheric temperatures. Another systematic change pattern which is obvious throughout all seasons, is found in mid-latitudes of the Northern Hemisphere (the pattern is obvious though less distinct in the Southern Hemisphere, as well). Here, the temperature change in the upper troposphere/lower stratosphere intensifies the zonal wind due to the thermal wind equation. This results in a more intense tropospheric jet stream in DJF and MAM, and tends to shift the jet stream to lower latitudes in JJA and SON. This

Title Page

Abstract | Introduction

Conclusions | References

Tables | Figures

◄ | ►

◄ | ►

Back | Close

Full Screen / Esc

Print Version

Interactive Discussion

EGU

is accompanied by a warming of the Arctic lower troposphere and a reduction of the horizontal temperature gradient at lower altitudes, resulting in a reduction of the zonal mean wind at around 50° to 60° N.

To display dynamical changes of the polar vortices during the 40 model years, an analysis of zonal mean temperature and zonal wind is presented in the style of the NCEP analyses (see NCEP web-page: http://code916.gsfc.nasa.gov/Data-services/ met/). Figure 9 shows climatological mean curves of the annual cycle of the zonal wind at 60°N and S at 30 hPa (Figs. 9a and 9c) and of the zonal mean temperature at 80° N and S at 30 hPa (Figs. 9b and 9d). The different lines represent mean values for the four decades covered by the transient simulation, the shaded area denotes the minimum and maximum values reached during the 1960s of the model. Similar to the results presented in Hein et al. (2001), the model again shows its ability to reproduce hemispheric differences of dynamical variability changes. While the annual cycle is well captured in both hemispheres, and the mean values in the Northern Hemisphere agree well with respective analyses derived from observations, the model has again deficiencies in the Southern Hemisphere, which are related to the cold bias (see discussion above). With regards to the dynamical variability of the Northern Hemisphere during winter and spring, E39/C shows reduced interannual variability in early winter. Nevertheless, E39/C is able to reproduce stratospheric warmings in mid and late winter, but the number of major events is smaller than observed. In the Northern Hemisphere the climatological mean values for the four decades do not indicate systematic changes (mainly due to the high dynamical variability), which is supported by analyses of observations (e.g. Labitzke and Naujokat, 2000). In the Southern Hemisphere the lower stratosphere do steadily change to more stable polar vortices and colder conditions in late winter and early spring. The lifetime (persistence) of the polar vortex has been prolonged by about three weeks, as the comparison of the results of the 1960s with those of the 1990s shows. This is in good agreement with an estimate presented by Zhou et al. (2000) who carried out their analysis on 19 years (1979–1998) of NCEP/NCAR reanalysis data and found that the Southern Hemisphere polar vortex has lasted about

EGU

two weeks longer in the 1990s than in the early 1980s.

3.3.   Tropopause and water vapour

Lower stratospheric water vapour trends may give a substantial contribution to the total radiative forcing of trace gas changes in the recent past (e.g. Rosenlof et al., 2001; Forster and Shine, 2002). However, time series analysis results from the few available observed data (e.g. Oltmans et al., 2000; Rosenlof et al., 2001; Randel et al., 2004) of stratospheric water vapour do not produce a uniform picture of the magnitude and even the sign of a respective trend. A possible feedback chain driving stratospheric water vapour trends involves trends in tropopause height (e.g. Steinbrecht et al., 2001; San-ter et al., 2003) and related tropopause temperature, which at least in the tropics may control changes in the water vapour penetration from the troposphere into the strato-sphere (Zhou et al., 2001). While in the present paper we will not investigate in detail the mechanisms responsible for long-term changes of water vapour concentrations in the lower stratosphere (a paper on this individual subject will be prepared later), we will give a brief overview of the overall trend simulated in the transient simulation.

The changes of the thermal tropopause pressure are given in Fig. 10a. Whereas no obvious systematic changes (trends) are seen in the first two decades of the simula-tion, model results indicate a gradual change in tropopause height after about 1980. In both hemispheres, E39/C simulates a decrease (increase) of tropopause pressure (height) poleward of around 50°. The subtropical regions show an increase (decrease) of tropopause pressure (height). There appears to be no uniform trend throughout the 40-year simulation in the tropics. The major volcanic eruptions included in the transient simulation lead to a temporary increase of tropopause pressure. Changes in tropopause temperature (not shown) are directly related to the variability of the tropopause height: An increase (decrease) of tropopause height goes along with a decrease (increase) of tropopause temperature. A comparison with an analysis of tropopause height changes at MOHp, 47.8° N (Steinbrecht et al., 1998; 2001) shows a qualitative agreement, i.e. a more or less steady increase of tropopause height in

EGU

Variability in a transient CCM simulation

M. Dameris et al.

February during the last 30 years. However, the model underestimates the rise in tropopause height compared to the estimates by Steinbrecht et al. (2001). Whereas Steinbrecht et al. finds an increase of +125 m/decade for the station MOHp, E39/C calculates only about +80 m/decade for the corresponding model grid point. A possible explanation for the rise of tropopause height could be the warming of the troposphere and the accompanying cooling of the stratosphere (Steinbrecht et al., 2001). If this would be the case, the difference between model results and observations can be explained by the fact, that tropospheric warming in the model at Northern Hemisphere mid-latitudes is smaller than observed (see discussion above).

Figure 10b depicts the changes of water vapour mixing ratio at the thermal tropopause during the 40 year model simulation. An uniform trend is obvious only in the subtropical region, where water vapour mixing ratios are higher in the late 1980s and the 1990s. Long-term changes are not uniform in the tropics, and neither at middle and high latitudes of both hemispheres. As discussed before, the volcanic eruptions involve characteristic signatures (see also below).

The general distribution of the change pattern in the lower stratosphere is equal to that at the tropopause. E39/C results, which allow a comparison with measurements of the Boulder frost point hygrometer and corresponding HALOE data discussed in Randel et al. (2004) (their Fig. 8a), are presented in Fig. 11 for the lower stratosphere (80 hPa). The figure shows not only the results at 40° N, but also at 40° S, since the temporal development is very similar.

A comparison between the measurement time series of stratospheric water vapour over Boulder (Oltmans et al., 2000) and the respective model data for the period after 1979 indicates a systematic model error with respect to the absolute concentration but good agreement with respect to the observed trend during these two decades (Stenke and Grewe, 2004). While the simulated stratospheric water vapour distribution could be significantly improved by including methane oxidation (e.g. Hein et al., 2001), it has also been established that the Boulder trend, as well as other observed trends during the 1990s are too strong to be explained by methane oxidation alone (Rosenlof, 2002).

Recently Joshi and Shine (2003) have been proposed that part of the observed long-term water vapour trend may be explained by the observed series of volcanic eruptions, provided that the stratospheric residence time of water vapour is in the order of 5 to 10 years and, thus, considerably longer than the residence time of the volcanic aerosols. Our model simulations do not reproduce this behaviour, as they indicate a memory of little more than 4 years at about 25 km height (Fig. 11).

Interestingly, E39/C simulates no positive trend in lower stratospheric water vapour mixing ratios in the years before 1980. On the contrary, a negative trend is found in the 1960s. A further discussion about possible reasons for this model behaviour is given in Sect. 4.3. Compared with the Boulder measurements one must conclude that the water vapour signals of the large volcanic eruptions are overestimated in E39/C (see discussion in Sect. 4.1). In addition, a more detailed analysis of stratospheric water vapour variability and trends involving further sensitivity studies with the model system is given in Stenke and Grewe (2004).

4. Variability due to external forcings

In this section, the model response to prescribed forcings is investigated. A guiding question for the discussion is, how deterministic the response of the non-linear atmospheric (model) system is. We consider both abrupt perturbations (e.g. volcanic eruptions) and quasi-periodic forcings like the QBO, the 10 to 12 year solar activity cycle, and fluctuating SSTs. This is important for a better understanding of the climate system to identify and quantify key parameters, which are most relevant for the description of atmospheric variability and changes and which, therefore, must form the focus of assessments of future atmospheric changes.

4.1. Volcanic eruptions

Major volcanic eruptions strongly disturb the atmosphere, as many analyses of observed physical, dynamical, and chemical parameters have shown (e.g. Coffey, 1996; Angell, 1997a,b; Andronova et al., 1999; Robock, 2000). Due to the upgraded observation techniques, the documentation of effects after the eruption of Mt. Pinatubo in 1991 is the most comprehensive. As described in Sect. 2, the transient simulation performed with E39/C considers the effects of volcanoes in the chemistry, as well as in the radiation scheme of the interactive model system.

Figure 12 shows a comparison of global mean temperature anomalies in the lower stratosphere derived from MSU Channel 4 (1979–2002) and equivalent temperatures (derived according to Santer et al., 1999) from the E39/C transient simulation (1960–1999). The most obvious features are the temperature increases immediately after the eruptions of Agung, El Chichon, and Mt. Pinatubo, which reach about 2 K in the simulation. The main part of the model signal originates from tropical latitudes, where maxima in the zonal mean response of more than 3 K occurs (not shown). Compared to the observed lower stratosphere temperature response following the eruptions of Agung, El Chichon and Mt. Pinatubo it is evident that the model response is overestimated by about 1 K (see also WMO, 1986). Kirchner et al. (1999) find a 2 K excess of their simulated temperature response (near the equator at 70 hPa, see their Fig. 5b) over observations, which they completely explain, by equal respective contributions of about 1 K, from the missing QBO modulation of heating rates and missing ozone depletion in their model configuration. As the QBO has been nudged into our transient experiment (see Sects. 2.2 and 4.2), no inconsistency to observations occurs in this respect. Likewise, the 1 K cooling effect that observed tropical ozone depletion forces on tropical temperatures according to Kirchner et al. (1999), should be included in our simulation in case that the interactive chemistry-climate coupling produces the correct signal. A reduction of tropical ozone similar to the observed one is indeed evident in the simulation (Fig. 4, compare with Bojkov and Fioletov (1995)). We can not con-

EGU

vincingly explain the apparent inconsistency between the conclusions of Kirchner et al. (1999) and our results, but some possibilities are conceivable: The vertical distribution of column ozone depletion may be different in both model systems, either due to shortcomings of the chemistry-climate model or because the diagnostic method used by Kirchner et al. (1999) was too simple. Similar differences may exist with respect to the QBO induced heating rates. A further possibility is the different water vapour feedback to be expected in both simulations: As the volcano-related heating of the tropical tropopause region is higher than observed in both simulations, but more distinct in the Kirchner et al. configuration, stratospheric water vapour uptake and its related radiative cooling feedback can be expected to be stronger in the simulations of Kirchner et al. (1999). If this is correct, the aerosol absorption heating rates calculated by Kirchner et al. (1999) for the Mt. Pinatubo eruption and adopted in our simulations may overestimate the actual effect after all, as they are able to balance an exaggerated water vapour radiative cooling in the original framework, but will overdo with respect to the smaller and more realistic water vapour feedback in the CCM simulation. A more speculative reason for the overestimation of the volcano signal is the possibility of injection of moist air masses from the volcano exhaust into the stratosphere that would not be modulated by freeze drying at the tropopause. If such contribution were substantial, a mechanism of moistening and cooling the stratosphere would be absent from both the simulations of Kirchner et al. (1999) and ours.

The heating of the stratosphere caused by volcanic aerosol results not only in an increase of the stratospheric mean temperature of about 2 K, it also enhances the meridional circulation. The vertical ascent in the tropics is amplified by roughly 20%, which results in an uplift of the ozone profile, i.e. a vertical displacement of the ozone maximum, and a decrease of the total ozone column of approximately 5% (Stenke and Grewe (2004); see also Fig. 4). The additional water vapour in the tropical lowermost stratosphere is significantly enhanced, which leads to an increase of OH by 20 to 25% at 70 hPa and a significantly stronger HO_x destruction cycle. However, chemical timescales in the lower stratosphere are still too large compared to the dynamical

timescale so that the chemical changes have only an impact on ozone in the order of 0.1% on the total column (Stenke and Grewe, 2004).

In northern mid-latitudes (40° N–50° N) at about 50 hPa ozone concentrations are not only dynamically controlled, but also by chemistry. Relative changes of ozone production and destruction cycles are similar during the three volcanic episodes, except for chlorine. Ozone production is reduced by 30% (Fig. 13a), which is strongly determined by heterogeneous conversion (on aerosol) from N_2O_5 to HNO_3 and by the reaction $NO+HO_2$ followed by photolysis of NO_2 in those regions in spring. Ozone loss rates show a more complex situation. The increase in water vapour leads to a more pronounced HO_x destruction in the order of 50% to 100% (not shown). The NO_x cycle is reduced by 20 to 40% due to a shift within the NO_y components, which results from the reaction $NO_2+OH\rightarrow HNO_3$. Ozone destruction by chlorine is doubled during the El Chichon period and even enhanced by a factor of 10 during the Pinatubo period compared to the non-volcanic period 1967 to 1979. In total, the enhanced ozone depletion by the HO_x cycle dominates during the Agung episode. During El Chichon, both the HO_x and ClO_x cycle are of equal importance. During the Pinatubo episode the changes in the destruction cycles are clearly dominated by the ClO_x cycle. This leads to an increased ozone destruction of around 20%, 40%, and 80% during the three volcanic episodes of Agung, El Chichon, and Mt. Pinatubo, respectively (Fig. 13a).

Using these changes in the production and loss rates, the effect on ozone is a reduction in the order of 5% per month at 50 hPa in the period March to May, based on a simple calculation applying the ozone production and loss terms from the climate-chemistry simulation. This leads to approximately 15% ozone loss at 50 hPa during spring related to the Pinatubo perturbation, which can be revealed by comparing early winter (November) and late spring (April) ozone values at 50 hPa (Fig. 13b). Both the November ozone values and the difference to the April ozone values are strongly perturbed during the post El Chichon and post Pinatubo period. Taking into account that 40% of the ozone column is affected by this process, then this reduces the ozone column by roughly 6%, which agrees with observational data (WMO, 2003).

Variability in a transient CCM simulation

M. Dameris et al.

EGU

The perturbation of dynamical and chemical values and parameters discussed so far lasted only for a relatively short time period of between 1.5 and 4 years. In addition, Fig. 12 indicates that the modelled temperature trend is in good agreement with the MSU analysis. Interestingly, similar to the changes derived from MSU data, the model results also indicate stepwise changes towards lower temperatures in the lower stratosphere after the eruptions of El Chichon and Mt. Pinatubo, which is not simulated after the eruption of Agung. No temperature trend is detected in the years after El Chichon and Pinatubo, neither in MSU analysis nor in E39/C data (see also Pawson and Naujokat, 1997). Dedicated additional simulations would be necessary for a conclusive interpretation, but a plausible explanation could be the following: The eruption of Agung happened during low solar activity whereas El Chichon and Mt. Pinatubo erupted shortly after and during solar maximum, respectively. The solar cycle effect probably masks the anticipated, more or less linear negative temperature trend, which is caused by enhanced concentrations of GHGs. Slightly enhanced (reduced) temperatures are expected in the lower stratosphere during higher (lower) solar activity due to higher (lower) short-wave heating rates (e.g. Matthes et al., 2004). The calculated temperature differences (i.e. annual, global mean) between solar maximum and minimum in the lower stratosphere (around 15 to 25 km) are approximately 0.2 K (Matthes et al., 2003), which is the same order of magnitude that is expected from the anthropogenic greenhouse effect. Therefore, in the years from 1985 to 1991 and after 1996 with increasing solar activity, the cooling of the lower stratosphere due to increasing concentrations of GHGs might be compensated such that no temperature trend is obvious.

4.2.   The quasi-biennial oscillation

Looking more carefully at the modelled temperature anomalies (Fig. 12), in particular in the years between 1965 and 1982, the QBO signal can be detected, which also contributes to the overall variability. A modulation of dynamical and chemical quantities caused by the prescribed QBO is also obvious in Fig. 4 in the equatorial region.

Variability in a transient CCM simulation

M. Dameris et al.

Title Page

Abstract	Introduction
Conclusions	References
Tables	Figures

◄◄ ►►

◄ ►

Back Close

Full Screen / Esc

Print Version

Interactive Discussion

EGU

Qualitatively, the QBO signal is in good agreement with a similar analysis derived from merged satellite and ground based data (Bojkov and Fioletov, 1995; updated version until the year 2000 is at our disposal, Fioletov, pers. communication). The anomalies derived from observations and the model results are of the same order of magnitude until the 1980s (i.e. up to 6%). They are notably smaller during the 1990s in E39/C, where observed fluctuations have continued with similar magnitudes. Here the modelled ozone varies only by about 2-3%. It seems that in E39/C the QBO signal in total ozone is partly masked by the (too) strong ozone anomalies after the volcanic eruptions. The QBO signal in E39/C can be detected in total ozone in all latitudinal regions. For example, at mid-latitudes of the Northern Hemisphere (Fig. 14), E39/C shows amplitudes in total ozone of 12 DU±4 DU during winter months (JFM) which can be clearly related to the QBO. Similar results have been found in an analysis based on TOMS data (Burrows et al., 2000; see also Fig. 2.4 in EC-report, 2001). A linear regression analysis of long-term measurements of ozone at MOHp, 47.8° N indicates QBO-related fluctuations of ± 10 DU (peak-to-trough ozone changes up to 20 DU) in February (Steinbrecht et al., 2001). The dominant effect of the QBO in the lower stratosphere is the variation of the meridional circulation and the tropical ascent. For example, in the case of a westerly jet (i.e. QBO east phase) the meridional circulation converges horizontally towards the jet core so that the upwelling is strongly reduced (increased) in the shear layer below (above) the jet. The opposite modification is found for the meridional circulation in the vicinity of the easterly jet. The QBO signal in tropical upwelling explains enhanced NO_y and reduced ozone and water vapour mixing ratios, all in the range of 5% to 10% around 50 hPa. Variations of lower stratospheric ozone depletion in the tropics caused by the QBO are in the order of ±15 to 20%. Positive (negative) ozone anomalies results in enhanced (reduced) NO_x and HO_x destruction cycles. This gives a clear indication that the variations of the destruction cycles are a consequence of the ozone variations and not vice versa, so that the QBO signal in column ozone is dynamically induced with some negative feedbacks from chemistry. Returning to Fig. 12, quasi-biennial fluctuations in the global mean temperature anomalies of the lower stratosphere are visible in

Title Page

Abstract | Introduction

Conclusions | References

Tables | Figures

◄ | ►

◄ | ►

Back | Close

Full Screen / Esc

Print Version

Interactive Discussion

EGU

the E39/C data, in particular in the years between 1966 and 1982, which is a long period without major volcanic activity. After the eruptions of El Chichon and Mt. Pinatubo a similar signature cannot be identified, neither in E39/C nor in the MSU data analysis.

4.3. The solar cycle

The impact of solar activity, in particular of the 11-year solar cycle, on climate and the stratosphere has often been investigated (e.g. Haigh, 1996). For example, total ozone anomalies have been estimated in the tropics (25° N to 25° S) for the years from 1978 to 2003 (WMO, 2003; Fig. 4-5 therein). This analysis was made on the basis of combined observations (synergistic use of ground-based and satellite data). It clearly shows strong decadal variations of total ozone in the tropics (approx. 3%), which indicates the link between long-term ozone variations especially in tropical regions and the activity cycle of the sun.

Our transient simulation includes the effects of changing photolysis rates below 30 km altitude and also chemically induced ozone changes caused by prescribed time evolution of NO_y at the model top. Calculated ozone anomalies in the tropical belt derived from E39/C (Fig. 15) develop similarly to observations (WMO, 2003), with positive anomalies around solar maximum (1981 and 1991) and negative anomalies around solar minimum (1986 and 1996). More sophisticated statistical analysis would be necessary to identify the solar cycle signal before 1978 where its presence is less but still suggested by higher ozone values around 1960 and 1969 in comparison to 1965. Note that the cycle between 1965 and 1976 has been less distinct, according to 10.7 cm radiation intensity records, than the other cycles included in the period. Recalling discussions in previous sections a distinct QBO signal is immediately evident in Fig. 15.

To get a better insight of the radiative impact of solar activity changes on dynamics and chemistry, it is helpful to have a look at the long-term variability of ozone photolysis and production rates during the 40 year transient simulation. Figure 16 shows respective results of E39/C at 10, 30, and 50 hPa at lower latitudes (25° N to 25° S).

The values calculated at 10 hPa directly reflect the prescribed changes of the extra-terrestrial flux at the upper boundary of E39/C, which is centred at 10 hPa. The solar signal can, to some part, still be identified at 30 hPa, the picture changes further down in the lower stratosphere. At 50 hPa, the 11-year solar cycle is no longer obvious be-cause of feedback processes (e.g. interactive ozone, influence of volcanic eruptions). Here, changes of ozone photolysis and production on longer time scales are identified, with minimum ozone photolysis and production rates in 1975 and higher values before and after this year. Interestingly, corresponding similar long-term changes are found in other model data sets: For example, in Sect. 3.3 it is shown that water vapour mix-ing ratios in mid-latitudes of the lower stratosphere slightly increase in the 1980s and 1990s, which is supported by observations at Boulder station (Oltmans et al., 2000). Model results for the 1970s indicate lowest water vapour mixing ratios without a visible trend and decreasing mixing ratios in the 1960s, whereas the values in the early 1960s are similar to those of the late 1990s. We explain these changes of water vapour mixing ratios with a corresponding behaviour of the cold-point temperature (not shown), which modifies the transport of water vapour from the troposphere into the stratosphere: A decrease of the cold-point temperature is found from 1960 until the early 1970s (i.e. around 1 K) and an increase of approximately 0.5 K is calculated from the beginning 1980s to 1999. Based on the currently available model results we speculate, although we cannot definitely conclude on the basis of this analysis, that long-term changes of the cold-point temperature are a consequence of solar activity fluctuations (i.e. via changes in photolysis rates, ozone production and concentration, net heating rates), although the coherence seems to be obvious.

Another parameter which has been reported to be influenced by long-term changes of solar activity is the duration of the stratospheric summer circulation at northern mid-and high latitudes (Offermann et al., 2004). Offermann et al. showed on the basis of meteorological analyses (e.g. NCEP, Berlin data) that the duration of summer (i.e. number of days with zonal mean east winds in 50° to 80° N and 60° to 80° S at 10 and 30 hPa) decreases in the 1980s and 1990s by about 10 to 20 days (depending

on latitude and altitude), whereas the length of summer increases in the 1960s and 1970s with the same order of magnitude. It seems plausible that the changes found in the 1980s and 1990s may have something to do with the anthropogenic greenhouse effect and the depletion of stratospheric ozone, which both lead to a more persistent polar vortex in winter. But this explanation does not hold for the description of changes found in the 1960s and 1970s. An analysis of summer duration in the E39/C transient simulation indicates a qualitatively similar behaviour as described in Offermann et al. (2004). On the basis of this result, we conclude that although solar activity is not the major driver of long-term changes of dynamical and chemical values and parameters in the lower stratosphere, it might have a stronger impact on stratospheric composition and circulation as previously expected.

We are aware that the evidence of solar variability effects in the transient simulation cannot be demonstrated convincingly by the few parameters reviewed here. Probably, as experience with conventional climate models without chemistry shows (e.g. Stott et al., 2002), an ensemble of transient simulations will be necessary to establish significant signals. This certainly holds for studies dealing with the proposed interaction between solar cycle and QBO to modify the northern hemisphere stratospheric circulation (Labitzke and van Loon, 1988). However, results presented here indicate that signals in chemical parameters (like water vapour and ozone) are likely to exist. Hence it appears promising to extend our coupled CCM studies with simulations using offline chemistry (e.g. Matthes et al., 2003) to clarify the role of chemical feedbacks for dynamical changes.

4.4. Summary and discussion

It is noteworthy to which extent the temporal and spatial development of atmospheric parameters in the transient E39/C CCM simulation matches with several observed features. On the one hand it is not surprising that the model is able to reasonably reproduce mean conditions and seasonal, interannual and long-term variability, since former investigations based on E39/C time-slice experiments (e.g. Hein et al., 2001; Schnadt

Title Page

Abstract | Introduction

Conclusions | References

Tables | Figures

◄ | ►

◄ | ►

Back | Close

Full Screen / Esc

Print Version

Interactive Discussion

EGU

et al., 2002; Austin et al., 2003) already indicate the capabilities of the coupled model system. On the other hand, it is not self-evident that a number of transient features and trends agree well in space and time with observations, especially as we have only one realisation of the 40-year time series available and, thus, could not reduce the stochastic component of the dynamics by ensemble averaging. The most remarkable examples are identified in the temporal development of ozone anomalies (Fig. 4): Consecutive cold and stable Northern Hemisphere winters in the stratosphere during the first half of the 1990s connected with low ozone columns; weak ozone hole events in 1986 and 1988; Southern Hemisphere mid-latitude anomalies in the years 1985, 1989, 1991/1992, and 1996. A possible explanation is that the prescribed SST, containing specific anomaly events (e.g. El Niño, La Niña), is a major driver for changes in planetary wave activity, which has a strong influence on the dynamics of the stratosphere, e.g. the Brewer-Dobson circulation. Additionally, the QBO filters waves propagating to the tropical stratosphere and modulates wave dynamics in the stratospheric wave guide. The reproduction of the positive water vapour trend in the lower stratosphere during the 1980s and 1990s is very encouraging for a more detailed study of the underlying cause and effect relationship. Changes in solar radiation due to the 11-year solar activity cycle is, evidently, another source for variations in the dynamical and chemical state of the simulated atmosphere, calling for specific sensitivity experiments.

The importance of the QBO and solar activity cycle for stratospheric dynamics has intensively been discussed for many years (e.g. Holton and Tan, 1980; Dameris and Ebel, 1990; Holton and Austin, 1991; Labitzke and van Loon, 2000). It is generally agreed that both influence to a large part the dynamical behaviour of the stratosphere, and therefore also the transport of tracers which impacts the chemical composition. The examples of E39/C results presented in this paper confirm that it is necessary to consider all major forcing mechanisms to obtain a realistic variability of dynamical and chemical values and parameters. The picture is not as suggestive for the role of the SST. Schnadt and Dameris (2003) showed that E39/C is able to reproduce the observed correlation of the North Atlantic Oscillation (NAO) pattern and the Northern

Variability in a transient CCM simulation

M. Dameris et al.

Title Page

Abstract	Introduction
Conclusions	References
Tables	Figures

◄ | ►|

◄ | ►

Back | Close

Full Screen / Esc

Print Version

Interactive Discussion

EGU

Hemisphere polar winter vortex: In the positive NAO phase the stratospheric vortex is stronger and colder than in the negative NAO phase. In the troposphere, the positive NAO phase is associated with an enhanced variance across the North Atlantic storm track whereas the negative NAO phase is suggestive of blocking. It was demonstrated that the vertical propagation of stationary (transient) planetary waves is reduced (enhanced) during the positive NAO phase, which clearly shows the link between SST and stratospheric dynamics. Multi-annual sensitivity simulations of 20 years each with the Met Office Unified Model have been investigated by Braesicke and Pyle (2004). For their experiments they changed the prescribed SSTs. They found that the appearance of extreme events in the Northern Hemisphere winter stratosphere is linked more to the representation of SSTs than it is to ozone. The significance of interannual variability in SSTs on stratospheric dynamics and ozone was demonstrated. Therefore, the underlying SST which is at least partly responsible for tropospheric circulation changes, certainly modifies the generation and propagation of planetary waves, which have an important influence on stratospheric dynamics.

5. Conclusions and outlook

The results discussed in this paper indicate where differences between model and observations are still obvious and where a detailed investigation of realistically simulated variability and trend components appear promising in order to improve the understanding of underlying processes and feedbacks. Such complementary investigations will be discussed in further papers, as they require a more dedicated and detailed analysis of correlations and interactions, also including parameters for which long-term observations are lacking. Additional sensitivity experiments with the same model system may also be required for such studies but considering the computational demands of CCMs those cannot be provided by the nick of time.

EGU

References

Andronova, N. G., Rozanov, E. V., Yang, F., and Schlesinger, M. E.: Radiative forcing by volcanic aerosols from 1850 to 1994, J. Geophys. Res., 104, 16 807–16 826, 1999. 2304, 2317

Angell, J. K.: Estimated impact of Agung, El Chichon, and Pinatubo volcanic eruptions on global and regional total ozone after adjustment for the QBO, Geophys. Res. Lett., 24, 647–650, 1997a. 2317

Angell, J. K.: Stratospheric warming due to Agung, El Chichon, and Pinatubo taking into account the quasi-biennial oscillation, J. Geophys. Res., 102, 9479–9485, 1997b. 2317

Austin, J.: A three-dimensional coupled chemistry-climate model simulation of past stratospheric trends, J. Atmos. Sci., 59, 218–232, 2002. 2299, 2300

Austin, J., Shindell, D., Beagley, S. R., Brühl, C., Dameris, M., Manzini, E., Nagashima, T., Newman, P., Pawson, S., Pitari, G., Rozanov, E., Schnadt, C., and Shepherd, T. G.: Uncertainties and assessments of chemistry-climate models of the stratosphere, Atmos. Chem. Phys., 3, 1–27, 2003,
SRef-ID: 1680-7324/acp/2003-3-1. 2300, 2302, 2325

Benkovitz, C. M., Scholtz, M. T., Pacyna, J., Tarrason, L., Dignon, J., Voldner, E. C., Spiro, P. A., Logan, J. A., and Graedel, T. E.: Global gridded inventories of anthropogenic emissions of sulfur and nitrogen, J. Geophys. Res., 101, 29 239–29 253, 1996. 2306

Bojkov, R. D. and Fioletov, V. E.: Estimating the global ozone characteristics during the last 30 years, J. Geophys. Res., 100, 16 537–16 551, 1995. 2309, 2317

Braesicke, P. and Pyle, J. A.: Sensitivity of dynamics and ozone to different representations of SSTs in the Unified Model, Q. J. R. Meteorol. Soc., 99, 1–9, 2004. 2326

Brühl, C. and Crutzen, P. J.: MPIC two-dimensional model, NASA Ref. Publ. 1292, 103–104, 1993. 2307

Burrows, J. P., Gleason, J., Labow, G., Eichmann, K.-U., Bramstedt, K., and Weber, M.: An

Variability in a transient CCM simulation

M. Dameris et al.

Title Page	
Abstract	Introduction
Conclusions	References
Tables	Figures

◄◄	►►
◄	►
Back	Close

Full Screen / Esc

Print Version

Interactive Discussion

EGU

overview of the stratosphere 1995-1999 as measured by GOME, Stratospheric Ozone 1999, Proceedings of the fifth European symposium, edited by: Harris, N. R. P., Guirlet, M., and Amanatidis, G. T., 27 September–1 October 1999, Saint Jean de Luz, France, Air Pollution Reseach Report No. 73, EUR 19340, ISBN 92-827-5672-6, 2000.

5   Chubachi, S.: A special ozone observation at Syowa Station, Antarctica from February 1982 to January 1983, Atmospheric Ozone: Proceedings of the Quadrennial Ozone Symposium, edited by: Zerefos, C. S. and Ghazi, A. M., Halkidiki, Greece, 3–7 September 1984, 285–289, 1985. 2308

Coffey, M. T.: Observations of the impact of volcanic activity on stratospheric chemistry, J. Geo-
10   phys. Res., 101, 6767–6780, 1996. 2317

Corbett, J.J., Fischbeck, P. S., and Pandis, S. N.: Global nitrogen and sulphur inventories for ocean-going ships, J. Geophys. Res., 104, 3457–3470, 1999. 2306

Dameris, M. and Ebel, A.: The quasi-biennial oscillation and major stratospheric warmings: A three-dimensional model study, Ann. Geophys., 8, 79–86, 1990. 2325

15   EC-report: European research in the stratosphere 1996–2000, Advances in our understanding of the ozone layer during THESEO, EUR 19867, ISBN 92-894-1398-0, 378, 2001.

Farman, J. C., Gardiner, B. G., and Shanklin, J. D.: Large losses of total ozone in Antarctica reveal seasonal ClO_x/NO_x interaction, Nature, 315, 207–210, 1985. 2308

Forster, P. M. de F. and Shine, K. P.: Assessing the climate impact of trends in stratospheric
20   water vapor, Geophys. Res. Lett., 29, doi:10.1029/2001GL013909, 2002. 2314

Fortuin, J. P. F. and Kelder, H.: An ozone climatology based on ozonesonde and satellite mea-surements, J. Geophys. Res., 103, 31 709–31 734, 1998. 2310

Fouquart, Y. and Bonnel, B.: Computation of solar heating of the Earth's atmosphere: A new parameterization, Beitr. Phys. Atmosph., 53, 35–62, 1980. 2306

25   Giorgetta, M. and Bengtsson, L.: Potential role of the quasi-biennial oscillation in the stratosphere-troposphere exchange as found in water vapor in general circulation model experiments, J. Geophys. Res., 104, 6003–6020, 1999. 2305

Grewe, V., Dameris, M., Hein, R., Sausen, R., and Steil, B.: Future changes of the atmospheric composition and the impact of climate change, Tellus, 53B, 103–121, 2001a. 2300

30   Grewe, V., Brunner, D., Dameris, M., Grenfell, J. L., Hein, R., Shindell, D., and Staehelin, J.: Origin and variability of upper tropospheric nitrogen oxides and ozone at northern mid-latitudes, Atmos. Environ., 35, 3421–3433, 2001b. 2301, 2302, 2311

Haigh, J.: The impact of solar variability on climate, Science, 272, 981–984, 1996. 2322

Variability in a transient CCM simulation

M. Dameris et al.

Title Page

Abstract	Introduction
Conclusions	References
Tables	Figures

◄◄   ►►

◄   ►

Back   Close

Full Screen / Esc

Print Version

Interactive Discussion

EGU

Hao, W. M., Liu, M.-H., and Crutzen, P. J.: Estimates of annual and regional releases of CO_2 and other trace gases to the atmosphere from fires in the tropics, based on the FAO statistics for the period 1975–1980, In: Fire in the Tropical Biota, Ecological Studies 84, edited by: Goldammer, J. G. , Springer-Verlag, New York, USA, 440–462, 1990. 2307

Hein, R., Crutzen, P. J., and Heimann, M.: An inverse modeling approach to investigate the global atmospheric methane cycle, Global Biogeochem. Cycles, 11, 43–76, 1997. 2306

Hein, R., Dameris, M., Schnadt, C., Land, C., Grewe, V., Köhler, I., Ponater, M., Sausen, R., Steil, B., Landgraf, J., Brühl, C.: Results of an interactively coupled atmospheric chemistry-general circulation model: Comparison with observations, Ann. Geophys., 19, 435–457, 2001,
SRef-ID: 1432-0576/ag/2001-19-435. 2301, 2302, 2309, 2310, 2313, 2315, 2324

Holton, J. R. and Tan, H.-C.: The influence of the equatorial quasi-biennial oscillation on the global circulation at 50 mb, J. Atmos. Sci., 37, 2200–2208, 1980. 2325

Holton, J. R. and Austin, J.: The influence of the equatorial QBO on sudden stratospheric warmings, J. Atmos. Sci., 48, 607–618, 1991. 2325

IPCC (Intergovernmental Panel on Climate Change): Special report on aviation and the global atmosphere, edited by: Penner, J. E., Lister, D. H., Griggs, D. J., Dokken, D. J., and McFarland, M., Cambridge University Press, Cambridge, United Kingdom and New York, NY, USA, 373, 1999. 2306, 2307

IPCC (Intergovernmental Panel on Climate Change): Climate change 2001: The scientific basis. Contribution of Working Group 1 to the Third Assessment Report, edited by: Houghton, J. T., Cambridge University Press, Cambridge, United Kingdom and New York, NY, USA, 881., 2001. 2306

Jackman, C. H., Fleming, E. L., Chandra, S., Considine, D. B., and Rosenfield, J. E.: Past, present, and future modeled ozone trends with comparisons to observed trends, J. Geophys. Res., 101, 28 753–28 767, 1996. 2303

Johnson, C. E., Collins, W. J., Stevenson, D. S., and Derwent, R. G.: The relative roles of climate and emission changes on future tropospheric oxidant concentrations, J. Geophys. Res., 104, 18 631–18 645, 1999. 2300

Joshi, M. M. and Shine, K. P.: A GCM study of volcanic eruptions as a cause of increased stratospheric water vapor, J. Clim., 16, 3525–3534, 2003. 2316

JPL (Jet Propulsion Laboratory): Chemical kinetics and photochemical data for use in stratospheric modeling: Evaluation 13. JPL-00-3, NASA Panel for Data Evaluation, NASA Aero-

Variability in a transient CCM simulation

M. Dameris et al.

nautics and Space Administration, Pasadena, CA, USA, 73, 2000. 2302

Junge, C., Chagnon, C., and Manson, J.: Stratospheric aerosols, J. Meteorol., 18, 81–108, 1961. 2304

Kirchner, I., Stenchikov, G. L., Graf, H.-F., Robock, A., and Antuna, J. C.: Climate model simulation of winter warming and summer cooling following the 1991 Mount Pinatubo volcanic eruption, J. Geophys. Res., 104, 19 039–19 055, 1999. 2304, 2317, 2318

Kurz, C. and Grewe, V.: Lightning and thunderstorms, Part I: observational data and model results, Meteorol. Z., 11, 379–393, 2002. 2302

Labitzke, K.: Stratospheric temperature changes after the Pinatubo eruption, J. Atmos. Terr. Phys., 56, 1027–1034, 1994. 2304

Labitzke, K. and van Loon, H.: Associations between the 11-year solar cycle, the QBO and the atmosphere, part I: The troposphere and stratosphere in the Northern Hemisphere in winter, J. Atmos. Terr. Phys., 50, 197–206, 1988. 2324

Labitzke, K. and Naujokat, B.: The lower arctic stratosphere in winter since 1952, SPARC Newsletter, 15, 11–14, 2000. 2313

Labitzke, K. and van Loon, H.: The QBO effect on the solar signal in the global stratosphere in the winter of the Northern Hemisphere, J. Atmos. Terr. Phys., 62, 621–628, 2000. 2325

Labitzke, K., et al.: The Berlin stratospheric data set, CD from Meteorological Institute, Free University Berlin, 2002. 2304

Lamago, D., Dameris, M., Schnadt, C., Eyring, V., and Brühl, C.: Impact of large solar zenith angles on lower stratospheric dynamical and chemical processes in a coupled chemistry-climate model, Atmos. Chem. Phys., 3, 1981–1990, 2003, SRef-ID: 1680-7324/acp/2003-3-1981. 2302, 2310

Land, C., Feichter, J., and Sausen, R.: Impact of vertical resolution on the transport of passive tracers in the ECHAM4 model, Tellus, 54B, 344–360, 2002. 2301

Landgraf, J. and Crutzen, P. J.: An efficient method for online calculations of photolysis and heating rates, J. Atmos. Sci., 55, 863–878, 1998. 2305

Lean, J., Rottmann, G., Kyle, H., Woods, T., Hickey, J., and Puga, L.: Detection and parameterisation of variations in solar mid- and near-ultraviolet radiation (200-400 nm), J. Geophys. Res., 102, 29 939–29 956, 1997. 2305

Manzini, E., Steil, B., Brühl, C., Giorgetta, M. A., and Krüger, K.: A new interactive chemistry climate model: 2. Sensitivity of the middle atmosphere to ozone depletion and increase in greenhouse gases and implications for recent stratospheric cooling, J. Geophys. Res., 108,

Variability in a transient CCM simulation

M. Dameris et al.

EGU

doi:10.1029/2002JD002977, 2003. 2299, 2300

Matthes, K., Kodera, K., Haigh, J. D., Shindell, D. T., Shibata, K., Langematz, U., Rozanov, E., and Kuroda, Y.: GRIPS solar experiments intercomparison project: Initial results, Pap. Meteorol. Geophys., 54, 71–90, 2003. 2320, 2324

5 Matthes, K., Langematz, U., Gray, L. L., Kodera, K., and Labitzke, K.: Improved 11-year solar signal in the Freie University Berlin climate middle atmosphere model, J. Geophys. Res., 109, doi:10.1029/2003JD004012, 2004. 2320

Matthes, S.: Globale Auswirkungen des Straßenverkehrs auf die chemische Zusammensetzung der Atmosphäre, PhD thesis, Ludwig-Maximilians Universität München, DLR-Report
10 2003-15, ISSN 1434-8454, 160, 2003. 2306

Mc Cormick, M. P., Thomason, L. W., and Trepte, C. R.: Atmospheric effects of the Mt. Pinatubo eruption, Nature, 373, 399–404, 1995. 2304

Mc Peters, R. D., Hollandsworth, S. M., Flynn, L. E., Herman, J. R., and Seftor, C. J.: Long-term ozone trends derived from the 16-year combined Nimbus 7/Meteor 3 TOMS version 7
15 record, Geophys. Res. Lett., 23, 3699–3702, 1996. 2310

Morcrette, J. J.: Radiation and cloud radiative properties in the European Centre for Medium Range Weather Forecasts forecasting system, J. Geophys. Res., 96, 9121–9132, 1991. 2306

Nagashima, T., Takahashi, M., Takigawa, M., and Akiyoshi, H.: Future development of the
20 ozone layer calculated by a general circulation model with fully interactive chemistry, Geophys. Res. Lett., 29, doi:10.1029/2001GL014026, 2002. 2299, 2300

Naujokat, B.: An update of the observed quasi-biennial oscillation of the stratospheric winds over the tropics, J. Atmos. Sci., 43, 1873–1877, 1986. 2304

Naujokat B. and Pawson, P.: The cold stratospheric winters 1994/1995 and 1995/1996, Geo-
25 phys. Res. Lett., 23, 3703–3706, 1996. 2308

Naujokat, B., Pawson, S., and Piel, A.: Is there a trend in the occurence of extremely low temperatures in the northern stratospheric winters? Proceedings of the first SPARC General Assembly, Melbourne, Australia, 2-6 December 1996, WCRP-99, WMO/TD-NO. 814, 157–160, 1997. 2308

30 Offermann, D., Donner, M., Knieling, P., and Naujokat, B.: Middle atmosphere temperature changes and the duration of summer, J. Atmos. Sol. Terr. Phys., 66, 437–450, 2004. 2323, 2324

Oltmans, S. J., Vömel, H., Hofmann, D. J., Rosenlof, K. H., and Kley, D.: The increase in strato-

Title Page	
Abstract	Introduction
Conclusions	References
Tables	Figures
◄◄	►►
◄	►
Back	Close
Full Screen / Esc	

Print Version

Interactive Discussion

EGU

spheric water vapor from balloonborne, frostpoint hygrometer measurements at Washington D.C., and Boulder, Colorado, Geophys. Res. Lett., 27, 3453–3456, 2000. 2314, 2315, 2323

Parker, D. E., Gordon, M., Cullum, D. P. N., Sexton, D. M. H., Folland, C. K., and Rayner, N.: A new global gridded radiosonde temperature data base and recent temperature trends, Geophys. Res. Lett., 24, 1499-1502, 1997. 2312

Pawson, S. and Naujokat, B.: Trends in daily wintertime temperatures in the northern stratosphere, Geophys. Res. Lett., 24, 575–578, 1997. 2320

Pawson, S. and Naujokat, B.: The cold winters of the middle 1990s in the northern lower stratosphere, J. Geophys. Res., 104, 14 209–14 222, 1999. 2308

Pawson, S., Kodera, K., Hamilton, K., et al.: The GCM-reality intercomparison project for SPARC (GRIPS): Scientific issues and initial results, Bull. Amer. Met. Soc., 81, 781–796, 2000. 2311

Pickering, K., Wang, Y., Tao, W.-K., Price, C., and Muller, F.-J.: Vertical distribution of lightning NO_x for use in regional and global chemical transport models, J. Geophys. Res., 103, 31 203–31 216, 1998. 2302

Pitari, G., Manzini, E., Rizi, V., and Shindell, D.: Impact of future climate and emission changes on stratospheric aerosols and ozone, J. Atmos. Sci., 59, 414–440, 2002. 2299, 2300

Price, C. and Rind, D.: A simple lightning parameterization for calculating global lightning distributions, J. Geophys. Res., 97, 9919–9933, 1992. 2302

Price, C. and Rind, D.: What determines the cloud-to-ground fraction of lightning in thunderstorms?, Geophys. Res. Lett., 20, 463–466, 1993. 2302

Randel, W. J. and Wu, F.: Cooling of the Arctic and Antarctic polar stratospheres due to ozone depletion, J. Climate, 12, 1467–1479, 1999. 2311

Randel, W. J., Wu, F., Oltmans, S. J., Rosenlof, K., and Nedoluha, G. E.: Interannual changes of stratospheric water vapor and correlations with tropical tropopause temperatures, J. Atmos. Sci., 61, 2133–2147, 2004. 2314, 2315

Rayner, N. A., Parker, D. E., Horton, E. B., Folland, C. K., Alexander, L. V., Rowell, D. P., Kent, E. C., and Kaplan, A.: Global analyses of sea surface temperatures, sea ice, and night marine air temperature since the late nineteenth century, J. Geophys. Res., 108, doi:10.1029/2002JD002670, 2003. 2303

Rex, M., Salawitch, R. J., von der Gathen, P., Harris, N. R. P., Chipperfield, M. P., and Naujokat, B.: Arctic ozone loss and climate change, Geophys. Res. Lett., 31, doi: 10.1029/2003GL018844, 2004. 2308

Variability in a transient CCM simulation

M. Dameris et al.

Robock, A.: Volcanic eruptions and climate, Rev. Geophys., 38, 191–219, 2000. 2304, 2317

Rosenfield, J., Considine, D., Meade, P., Bacmeister, J., Jackman, C., and Schoeberl, M.: Stratospheric effects of Mount Pinatubo aerosol studied with a coupled two-dimensional model, J. Geophys. Res., 102, 3649–3670, 1997. 2303

Rosenlof, K. H., Oltmans, S. J., Kley, D., Russell III, J. M., Chiou, E.-W., Chu, W. P., Johnson, D. G., Kelly, K. K., Michelsen, H. A., Nedoluha, G. E., Remsberg, E. E., Toon, G. C., and McCormick, M. P.: Stratospheric water vapor increases over the past half-century, Geophys. Res. Lett., 28, 1195–1198, 2001. 2314

Rosenlof, K. H.: Transport changes inferred from HALOE water and methane measurements, J. Meteorol. Soc. Japan, 80, 831–848, 2002. 2315

Rozanov, E. V., Schlesinger, M. E., and Zubov, V. A.: The Universtiy of Illinois at Urbana-Champaign three-dimensional stratosphere-troposphere general circulation model with interactive ozone photochemistry: Fifteen-year control run climatology, J. Geophys. Res., 106, 27 233–27 254, 2001. 2299, 2300

Santer, B. D., Hnilo, J. J., Wigley, T. G., Boyle, J. S., Doutriaux, C., Fiorino, M., Parker, D. E., and Taylor, K. E.: Uncertainties in observationally based estimates of temperature change in the free atmosphere, J. Geophys. Res., 104, 6305–6333, 1999. 2317

Santer, B. D., Wehner, M. F., Wigley, T. G., Sausen, R., Meehl, G. A., Taylor, K. E., Ammann, C., Arblaster, J., Washington W. M., Boyle, J. S., and Brüggemann, W.: Contributions of anthropogenic and natural forcing to recent tropopause height changes, Science, 301, 479–483, 2003. 2314

Sato, M., Hansen, J. E., McCormick, M. P., and Pollack, J. B.: Stratospheric aerosol optical depths, 1850-1990, J. Geophys. Res., 98, 22 987–22 994, 1993. 2304

Schmitt, A., and Brunner, B.: Emissions from aviation and their development over time, in Pollutants from air traffic – results of atmospheric research 1992–1997, DLR-Mitt. 97-04, U. Schumann et al. (Eds.), 37–52, DLR Köln, Germany, 1997. 2306

Schnadt, C., Dameris, M., Ponater, M., Hein, R., Grewe, V., and Steil, B.: Interaction of atmospheric chemistry and climate and its impact on stratospheric ozone, Clim. Dyn., 18, 501–517, 2002. 2299, 2300, 2301, 2311, 2324

Schnadt, C. and Dameris, M.: Relationship between North Atlantic Oscillation changes and stratospheric ozone recovery in the northern hemisphere in a chemistry-climate model, Geophys. Res. Lett., 30, doi:10.1029/2003GL017006, 2003. 2325

Shine, K. P., Bourqui, M.S., Forster, P. M. F., Hare, S. H. E., Langematz, U., Braesicke, P.,

Variability in a transient CCM simulation

M. Dameris et al.

Title Page

Abstract	Introduction
Conclusions	References
Tables	Figures

◄◄ ►►

◄ ►

| Back | Close |

Full Screen / Esc

Print Version

Interactive Discussion

EGU

Grewe, V., Ponater, M., Schnadt, C., Smith, C. A., Haigh, J. D., Austin, J., Butchart, N., Shindell, D. T., Randel, W. J., Nagashima, T., Portmann, R. W., Solomon, S., Seidel, D. J., Lanzante, J., Klein, S., Ramaswamy, V., and Schwarzkopf, M. D.: A comparison of model-simulated trends in stratospheric temperatures, Quart. J. R. Met. Soc., 129, 1565–1588, 2003. 2312

Steil, B., Dameris, M., Brühl, C., Crutzen, P. J., Grewe, V., Ponater, M., and Sausen, R.: Development of a chemistry module for GCMs: first results of a multiannual integration, Ann. Geophys., 16, 205–228, 1998, SRef-ID: 1432-0576/ag/1998-16-205. 2301

Steil, B., Brühl, C., Manzini, E., Crutzen, P. J., Lelieveld, J., Rasch, P. J., Roeckner, E., and Krüger, K.: A new interactive chemistry climate model: 1. Present day climatology and inter-annual variability of the middle atmosphere using the model and 9 years of HALOE/UARS data, J. Geophys. Res., 108, doi:10.1029/2002JD002971, 2003. 2299, 2300

Steinbrecht, W., Claude, H., Köhler, U., and Hoinka, K. P.: Correlations between tropopause height and total ozone: implications for long-term changes, J. Geophys. Res., 103, 19 183–19 192, 1998. 2312

Steinbrecht, W., Claude, H., Köhler, U., and Winkler, P.: Interannual changes of total ozone and northern hemisphere circulation patterns, Geophys. Res. Lett., 28, 1191–1194, 2001. 2314, 2315, 2321

Stenke, A. and Grewe, V.: Simulation of stratospheric water vapour trends: Impact on strato-spheric ozone chemistry, Atmos. Chem. Phys. Disscuss., 4, 6559–6602, 2004. 2315, 2316, 2318, 2319

Stott, P. A., Tett S. F. B., Jones, G. S., Allen, M. R., Mitchell, J. F. B., and Jenkins, G. J.: External control of twentieth century temperature variations by natural and anthropogenic forcings, Science, 15, 2133–2137, 2002. 2324

Wang, C. and Prinn, R. G.: Impact of emissions, chemistry, and climate on atmospheric carbon monoxide: 100-year predictions from a global chemistry-climate model, Chemosphere Global Change Science, 1, 77–81, 1999. 2300

WMO (World Meteorological Organisation): Atmospheric Ozone 1985, Global Ozone Research and Monitoring Project, Report No. 16, 1986. 2317

WMO (World Meteorological Organisation): Scientific Assessment of Ozone depletion: 1999, Global Ozone Research and Monitoring Project, Report No. 44, ISBN 92-807-1722-7, 1999. 2312

Variability in a transiant CCM simulation

M. Dameris et al.

Title Page

Abstract	Introduction
Conclusions	References
Tables	Figures

|◄ | ►|

◄ | ►

Back | Close

Full Screen / Esc

Print Version

Interactive Discussion

EGU

WMO (World Meteorological Organisation): Scientific Assessment of Ozone depletion: 2002, Global Ozone Research and Monitoring Project, Report No. 47, ISBN 92-807-2261-1, 2003. 2303, 2307, 2319, 2322

Yienger, J. J. and Levy II, H.: Empirical model of global soil-biogenic NO_x emissions, J. Geophys. Res., 100, 11 447–11 464, 1995. 2307

Zhou, S., Gelman, M. E., Miller, A. J., and McCormack, J. P.: An inter-hemispheric comparison of the persistent stratospheric polar vortex, Geophys. Res. Lett., 27, 1123–1126, 2000. 2313

Zhou, X.L., Geller, M. A., and Zhang, M. H.: Tropical cold point tropopause characteristics derived from ECMWF reanalysis and soundings, J. Clim., 14, 1823–1838, 2001. 2314

Variability in a transient CCM simulation

M. Dameris et al.

Title Page

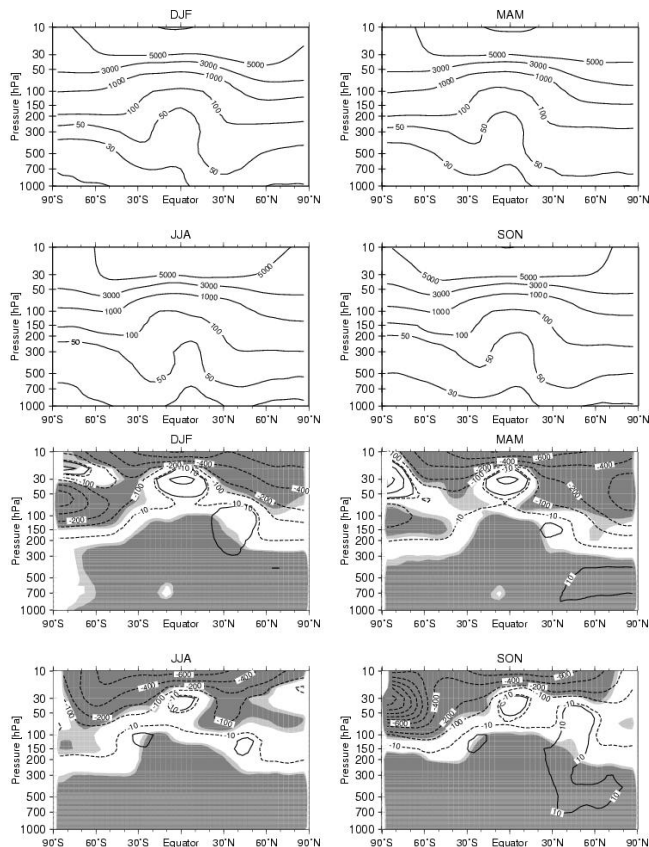| Abstract | Introduction |
| Conclusions | References |
| Tables | Figures |

|◄ | ►|

◄ | ►

Back | Close

Full Screen / Esc

Print Version

Interactive Discussion

EGU

EGU

Table 1. Overview of the external forces included in the transient model simulation.

Forcing	Circulation	Chemistry
SST	Real observations – GISS/Hadley	–
Volcanoes	Simulated heating rates	Observed/estimated SADs from SAGE
QBO	Zonal stratospheric tropical winds "nudged" towards observations	–
Solar Cycle	Changes in the solar constant	Changes in extra-terrestrial fluxes (7 bands) affecting photolysis rates
CO_2	Greenhouse gas	–
CH_4, N_2O, CFCS	Greenhouse gases	Reaction with OH/photolysis impacts strat. and trop. chemistry
NO_x emissions	–	Impact on ozone chemistry

Table 2. Total intensity (solar constant, in W/m^2) and extra-terrestrial fluxes (in phot/cm^{2}s) at the uppermost model level, as assumed in E39/C. The spectral intervals are given in nm. The values for solar maximum represent values measured in the year 1991.

	value in solar minimum	value in solar maximum	difference
total intensity [W/m^2]	1365.00	1366.09	1.09
extra-terrestrial flux at 10 hPa (phot/cm^{2}s)			
178.8–202.0	$8.80 \cdot 10^{12}$	$9.67 \cdot 10^{12}$	$0.87 \cdot 10^{12}$
202.0–241.0	$1.70 \cdot 10^{14}$	$1.77 \cdot 10^{14}$	$0.70 \cdot 10^{13}$
241.0–289.9	$1.12 \cdot 10^{15}$	$1.14 \cdot 10^{15}$	$0.22 \cdot 10^{14}$
289.9–305.5	$1.27 \cdot 10^{15}$	$1.28 \cdot 10^{15}$	$0.05 \cdot 10^{14}$
305.5–313.5	$7.97 \cdot 10^{14}$	$8.01 \cdot 10^{14}$	$0.36 \cdot 10^{13}$
313.5–337.5	$3.36 \cdot 10^{14}$	$3.36 \cdot 10^{14}$	0.
337.5–422.5	$2.06 \cdot 10^{16}$	$2.06 \cdot 10^{16}$	0.
422.5–752.5	$1.29 \cdot 10^{17}$	$1.29 \cdot 10^{17}$	0.

[EGU](#)
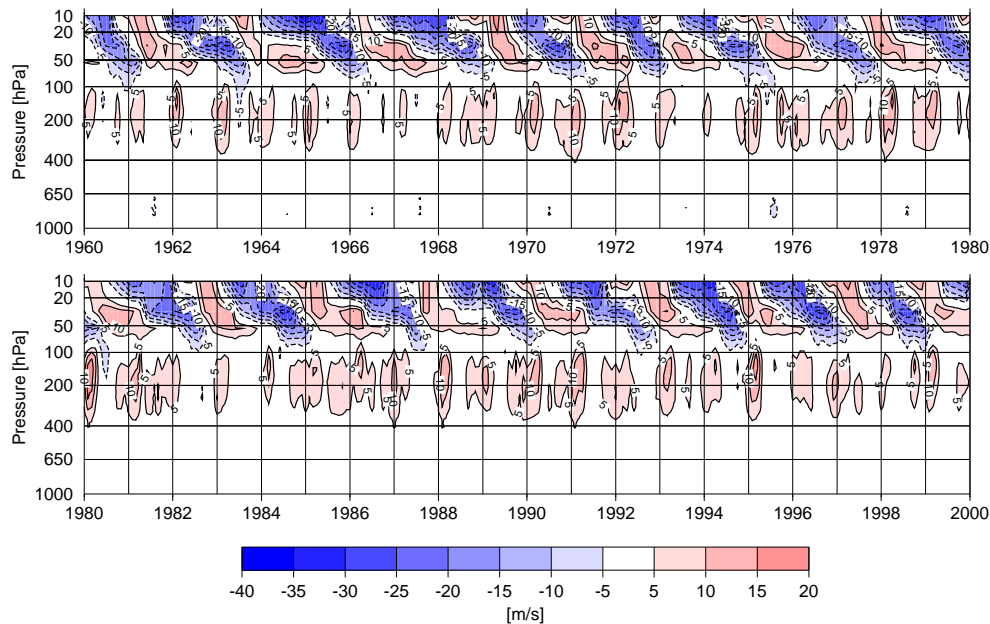
Fig. 1. Assimilated monthly mean zonal winds (in m/s) near the equator (zonal mean values) in the E39/C model simulation. Negative (positive) wind speed indicates easterly (westerly) wind.

Variability in a transient CCM simulation

M. Dameris et al.

EGU
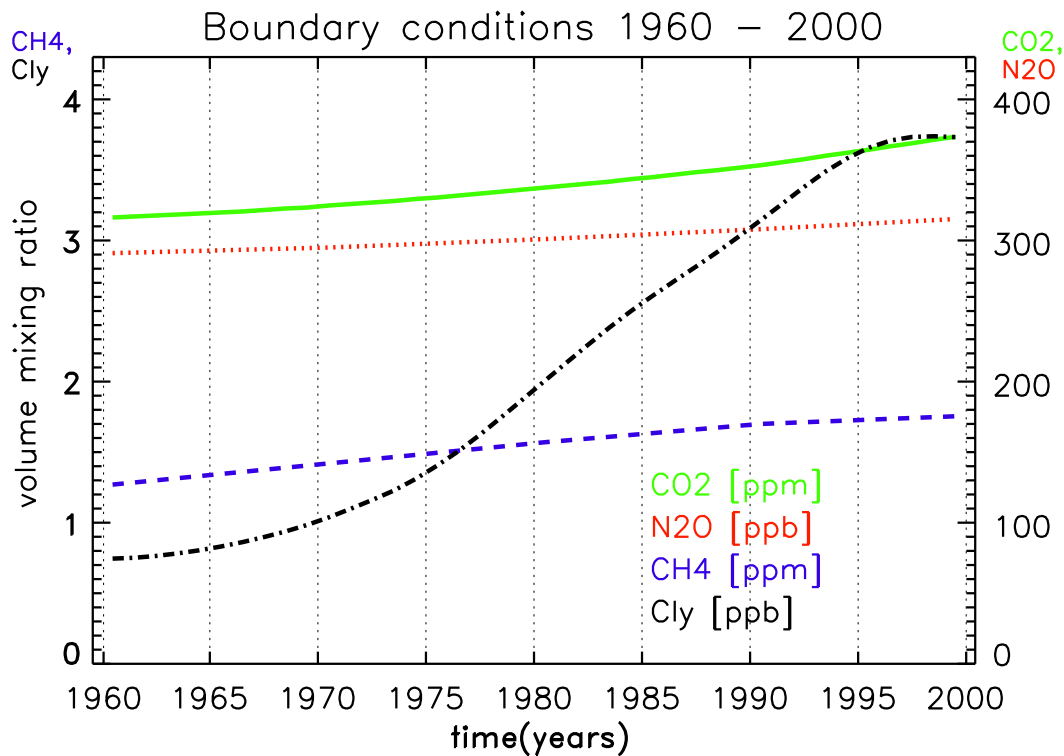
Fig. 2. Changes of mixing ratios of CO_2 (in ppmv), N_2O (in ppbv), CH_4 (in ppmv), and Cl_y (in ppbv), as adopted in the transient simulation with E39/C.

Variability in a transient CCM simulation

M. Dameris et al.

Title Page

Abstract	Introduction
Conclusions	References
Tables	Figures

I◀	▶I
◀	▶
Back	Close

Full Screen / Esc

Print Version

Interactive Discussion

EGU
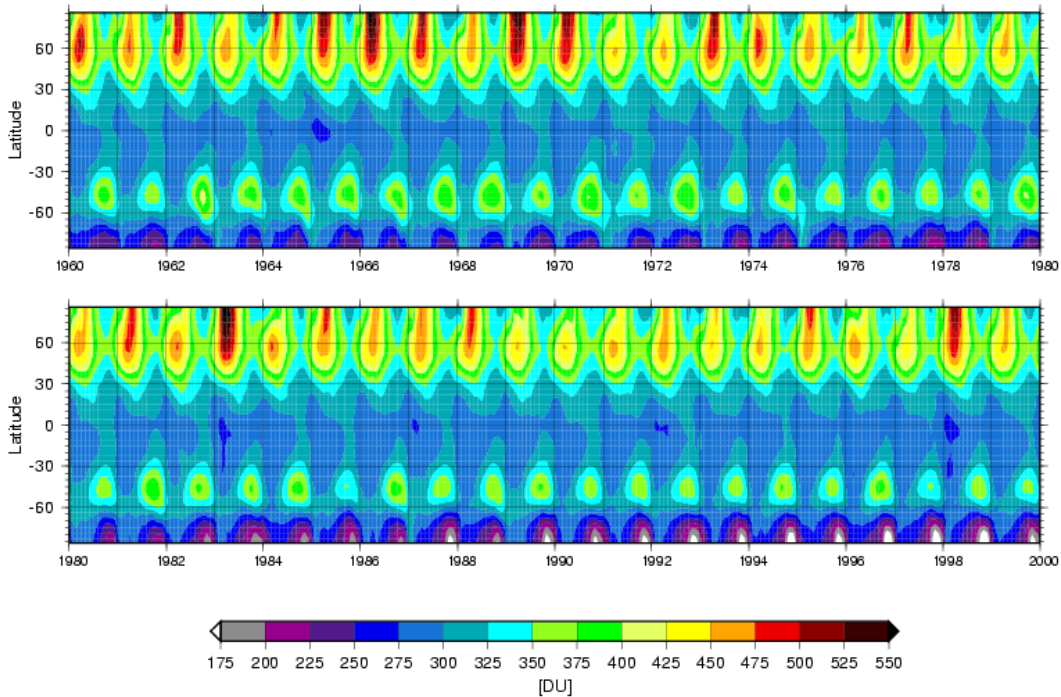
Fig. 3. Development of monthly mean total ozone between 1960 and 1999, as calculated with E39/C. The zonal mean values are given in Dobson Units (DU).

Variability in a transient CCM simulation

M. Dameris et al.

EGU
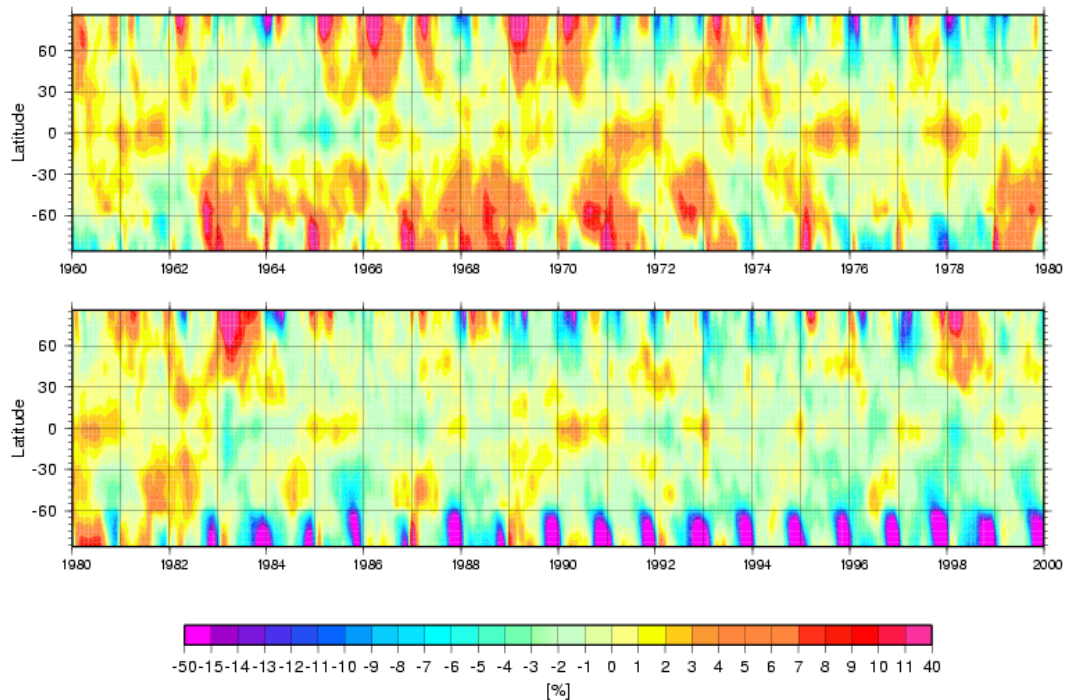
Fig. 4. Anomalies of total ozone relative to associated mean values derived for the period between 1964 and 1980. Positive (negative) values (in %) indicate more (less) ozone with regards to the reference period.

(a)

(c)

(b)

(d)
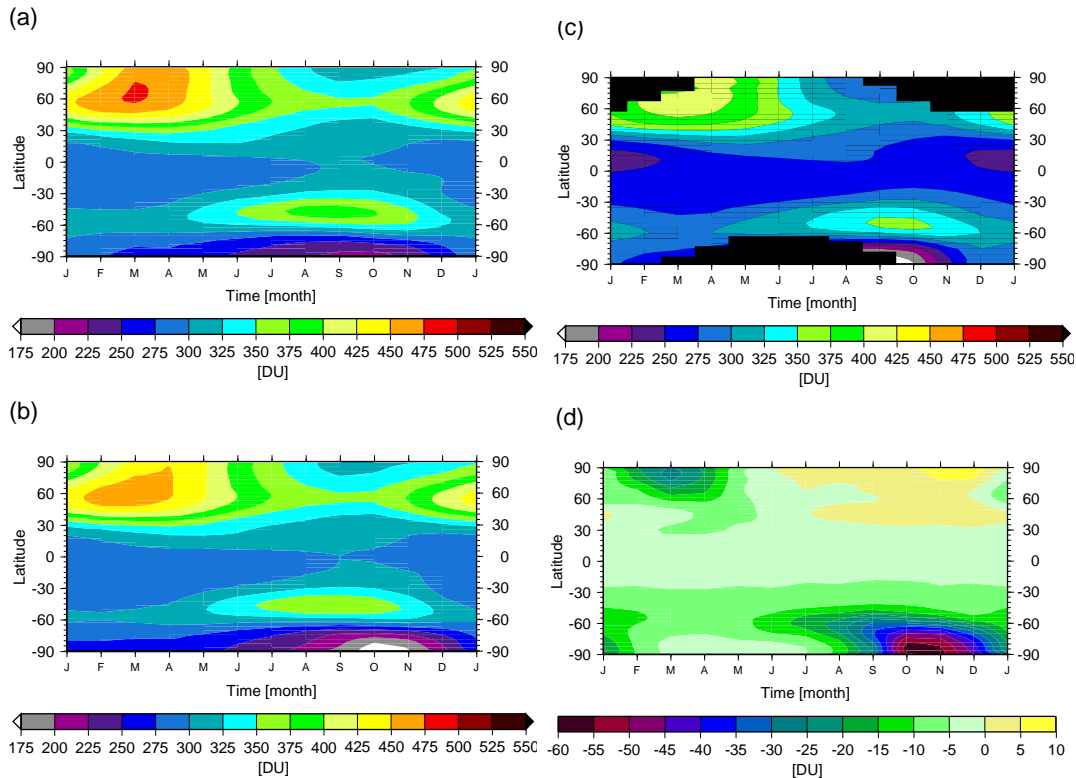
Fig. 5. Climatologies of total ozone derived from E39/C for the periods 1960 to 1979 **(a)**, 1980 to 1999 **(b)**, and from TOMS measurements during the years from 1980 to 1999 **(c)**. Differences between the two E39/C climatologies are displayed in **(d)**, where positive (negative) values indicate more (less) ozone in second half of the 40-year transient simulation. Given values are in DU.

Title Page

Abstract | Introduction

Conclusions | References

Tables | Figures

|◄ | ►|

◄ | ►

Back | Close

Full Screen / Esc

Print Version

Interactive Discussion

EGU

Fig. 6. Top: Seasonal mean values of zonal mean ozone mixing ratios derived from E39/C transient simulation for the 1960s (1960 to 1969). Bottom: Differences calculated between mean values derived for the 1960s and corresponding values for the 1990s. Positive (negative) values indicate more (less) ozone in the 1990s. Light (dark) shading indicates regions in which differences are statistically significant at the 95% (99%) level (t-test). Units are in ppbv.
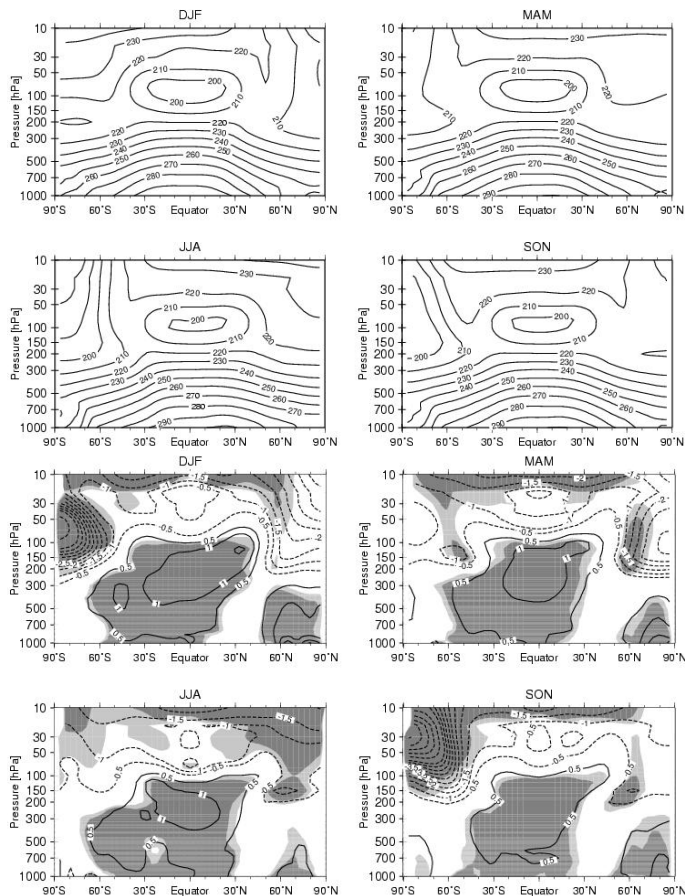
Fig. 7. Same as in Fig. 6, but for temperature. Positive (negative) values indicate higher (lower) temperature in the 1990s. Units are in K. The interval of contour lines is 0.5 K, minimum values in the southern polar stratosphere are −5.5 K in DJF and −7.0 K in SON.
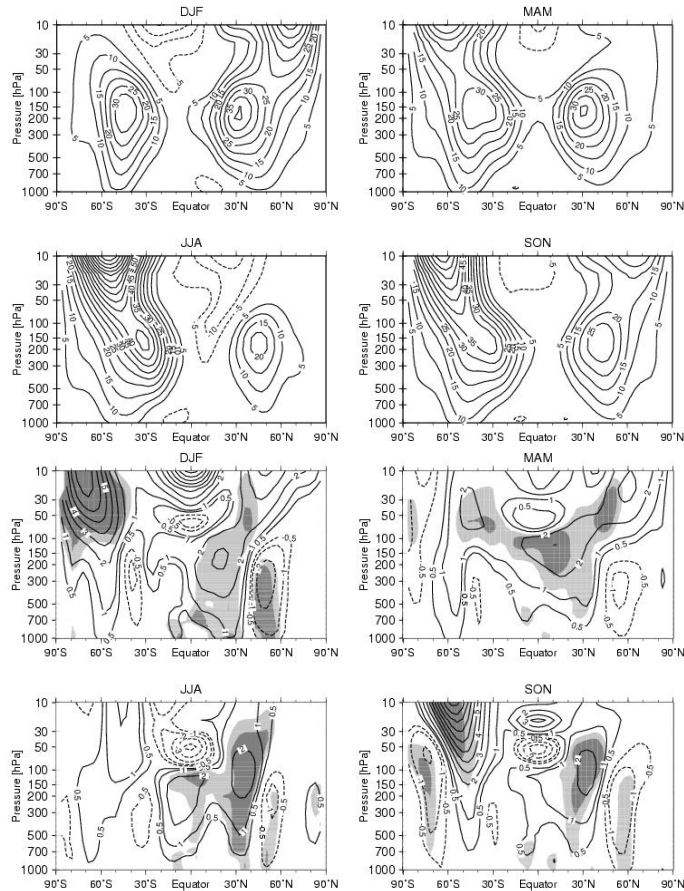
Fig. 8. Same as in Fig. 6, but for zonal wind. Positive (negative) values indicate higher (lower) wind speed in the 1990s. Units are in m/s. The interval of contour lines is 1 m/s plus the 0.5 and −0.5 contour lines, maximum values in the southern stratosphere are 7 m/s in DJF and 10 m/s in SON.

EGU
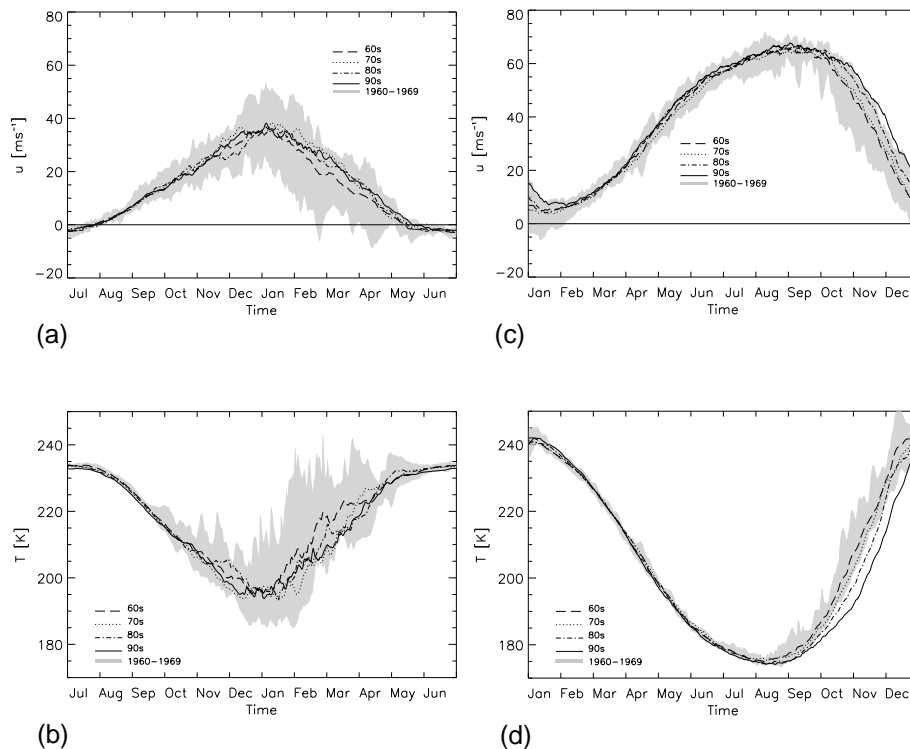
Fig. 9. Climatological mean curves of the annual cycle of the zonal wind (in m/s) at 60° N **(a)** and 60°S **(c)** at 30 hPa, and of the zonal mean temperature (in K) at 80° N **(b)** and 80° S **(d)** at 30 hPa. Different lines indicate decadal mean values of the four decades, i.e. the 1960s, 1970s, 1980s, and 1990s. The shaded areas show the range of minimum and maximum values found within the 1960s.

Variability in a transient CCM simulation

M. Dameris et al.

EGU
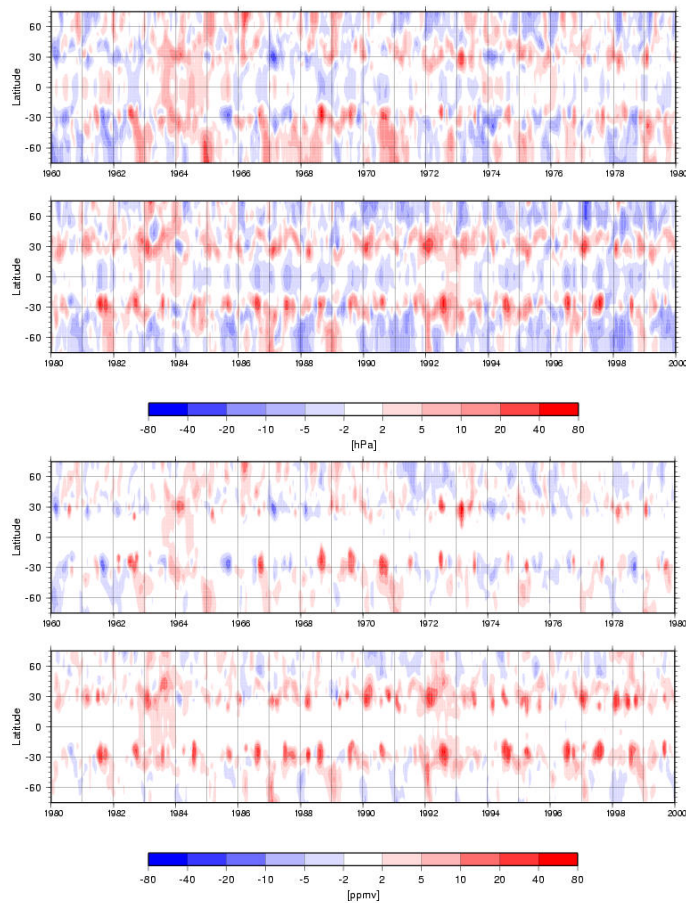
Fig. 10. Zonal mean changes of pressure (in hPa, top panel) and of water vapour mixing ratio (in ppmv, bottom panel) at the thermal tropopause, as simulated with E39/C.

2347

EGU
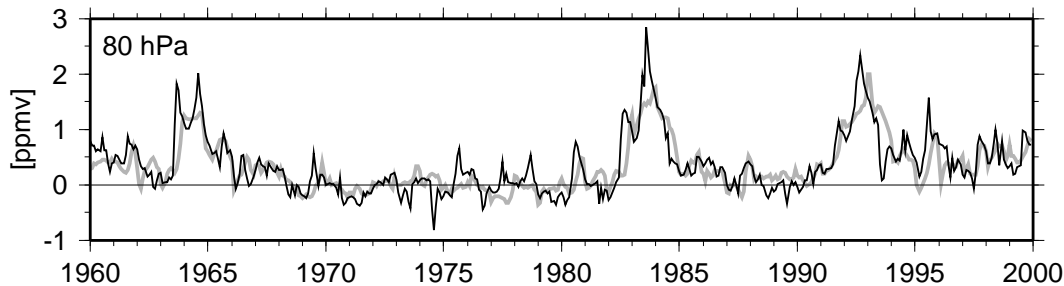
Fig. 11. Temporal development of zonal mean water vapour anomalies (in ppmv) at 40° N (black curve) and 40° S (grey curve) at 80 hPa as simulated with E39/C. The given values of differences are with respect to reference values of the years 1960 to 1980.

EGU
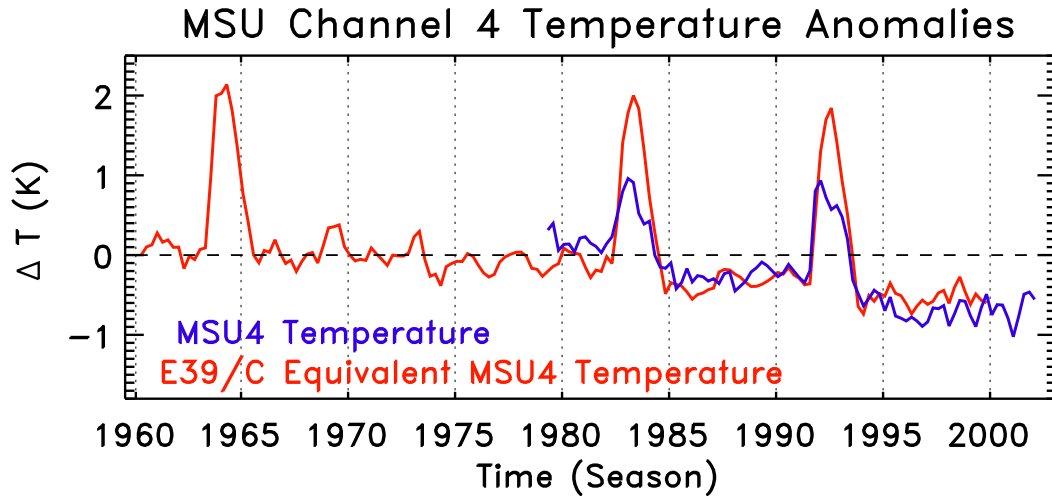
Fig. 12. Comparison of global mean temperature anomalies in the lower stratosphere (15 to 23 km) derived from observations (MSU Channel 4) and equivalent values calculated from results of the E39/C model simulation.
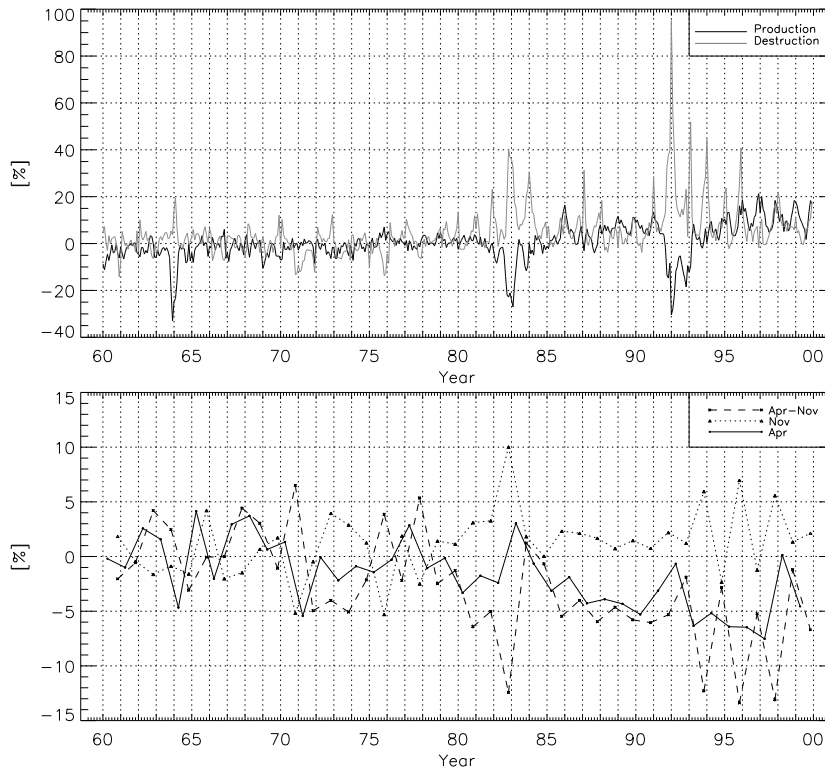
Fig. 13. Top: Monthly mean deviation of O_3 production and O_3 destruction at 50.1° N, 50 hPa. The deviation has been calculated separately for each month, relative to the associated reference month, as a climatologiocal mean for 1967–1979. Bottom: Monthly mean deviation of O_3 concentration for the months April, November, and the difference April–November at 50.1° N, 50 hPa. The deviation has been calculated separately for April and November, relative to the associated reference month as a climatologiocal mean for 1967–1979.

Title Page

Abstract | Introduction

Conclusions | References

Tables | Figures

◀ | ▶

◀ | ▶

Back | Close

Full Screen / Esc

Print Version

Interactive Discussion

EGU

EGU
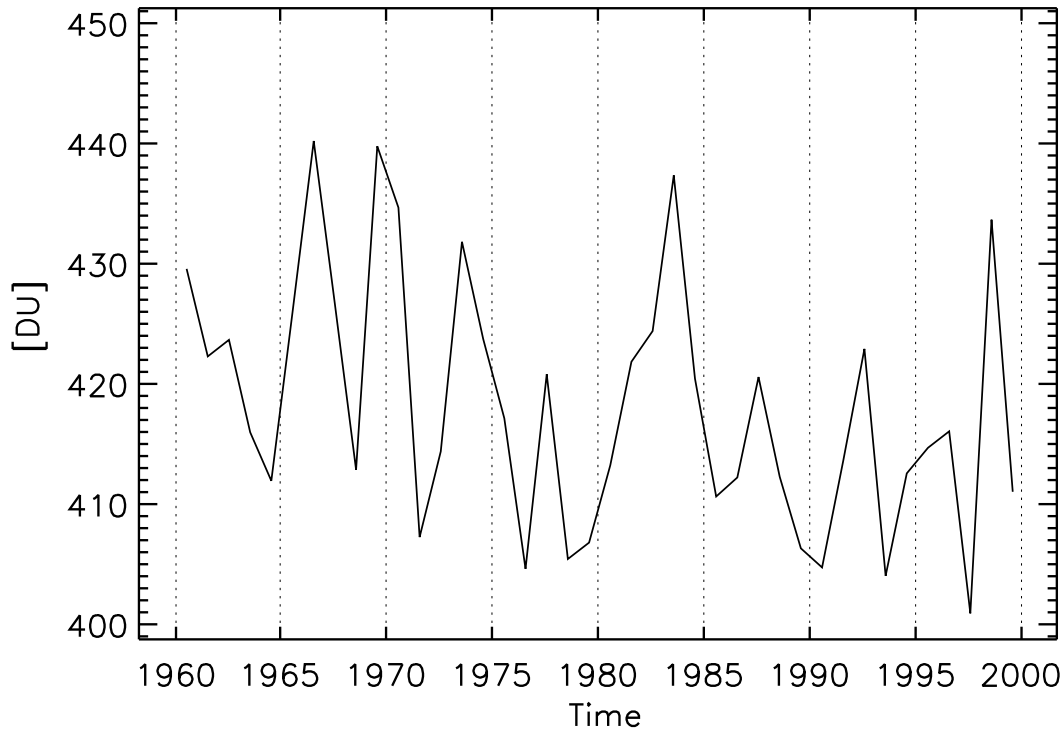
Fig. 14. Temporal development of total ozone for the midlatitude region of 30° N and 60° N, calculated for January, February, and March averages, derived from E39/C model results. Values are given in DU.
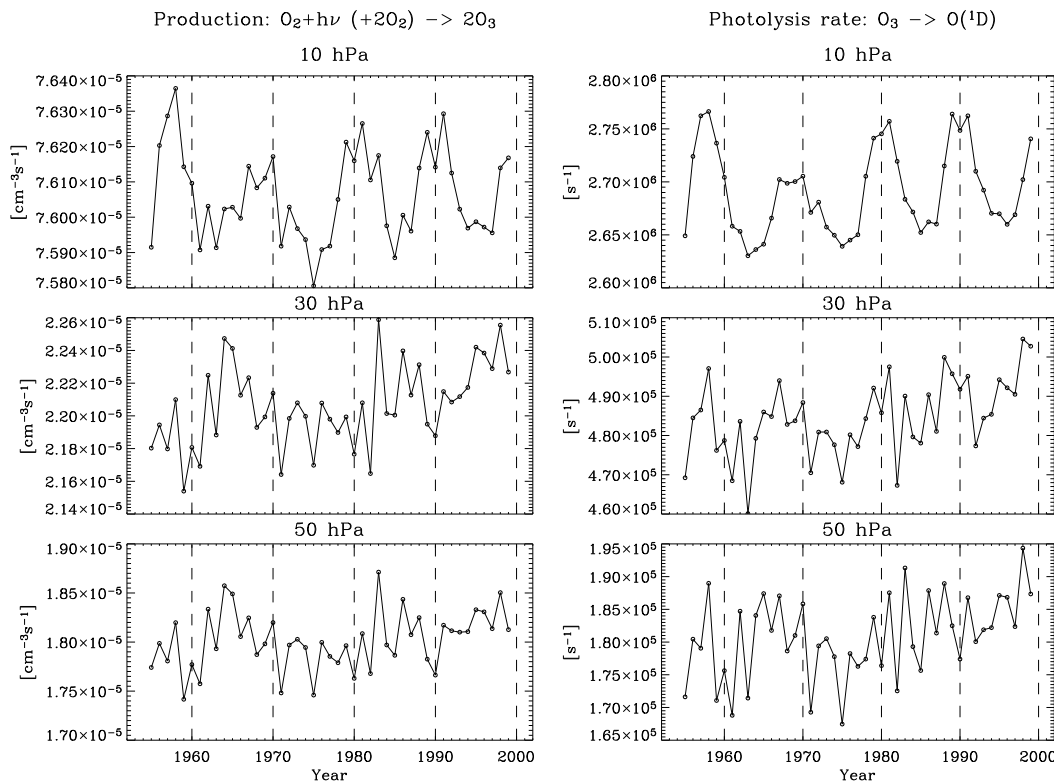
EGU
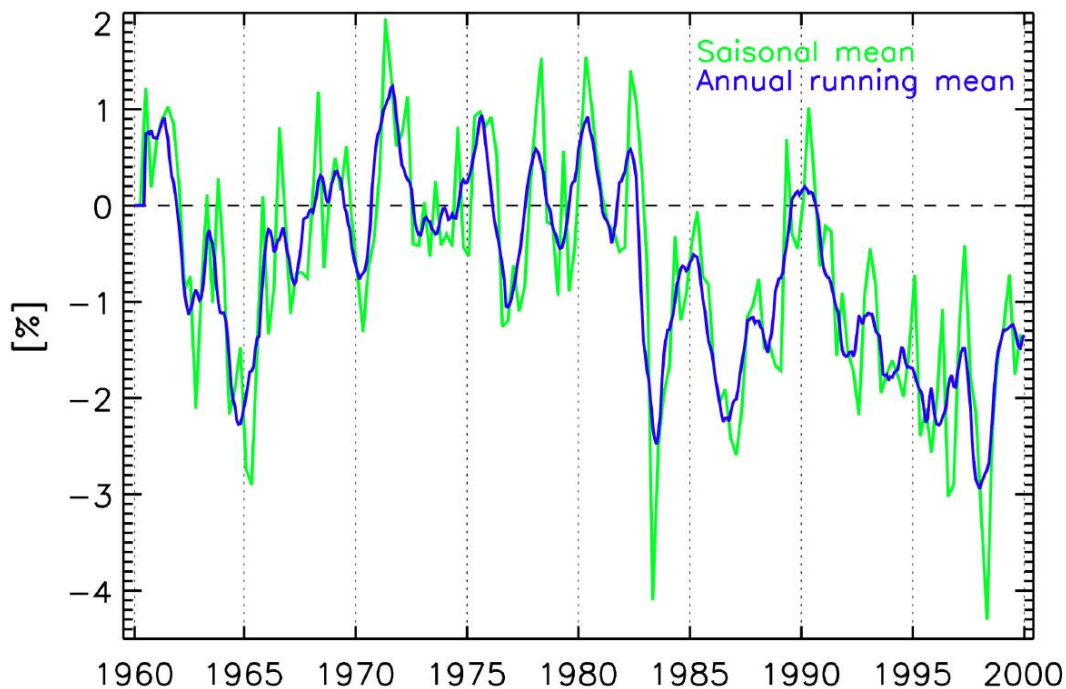
Fig. 15. Total ozone deviations (in %) for the latitude range 25° S to 25° N. Anomalies are calculated from E39/C results with respect to the model data during the years 1964 to 1980.

Production: $O_2 + h\nu$ $(+2O_2)$ $\rightarrow$ $2O_3$

Photolysis rate: $O_3 \rightarrow O(^1D)$

Fig. 16. Temporal development of ozone production rates (left, in $cm^{-3}s^{-1}$) and ozone photolysis rates (right, in s^{-1}) at 10 hPa (top), 30 hPa (middle), and 50 hPa (bottom), for the latitude range 25° S to 25° N.